



**CHALMERS**  
UNIVERSITY OF TECHNOLOGY

---

# **Synthesis and Quality Control of Radiohalogenated PSMA Inhibitors**

for Targeted Therapy of Prostate Cancer

Master's thesis in Nuclear Engineering

Tierra Duffield



MASTER'S THESIS 2015

# Synthesis and Quality Control of Radiohalogenated PSMA Inhibitors

for Targeted Therapy of Prostate Cancer

TIERRA DUFFIELD



**CHALMERS**  
UNIVERSITY OF TECHNOLOGY

Department of Nuclear Engineering  
Targeted Alpha Therapy Group  
CHALMERS UNIVERSITY OF TECHNOLOGY  
Gothenburg, Sweden 2015

Synthesis and Quality Control of Radiohalogenated PSMA Inhibitors  
for Targeted Therapy of Prostate Cancer  
TIERRA DUFFIELD

© TIERRA DUFFIELD, 2015.

Supervisor: Sture Lindegren, Department of Radiation Physics, Sahlgrenska  
Examiner: Christian Ekberg, Department of Nuclear Chemistry

Master's Thesis 2015  
Department of Nuclear Engineering  
Targeted Alpha Therapy Group  
Chalmers University of Technology  
SE-412 96 Gothenburg  
Telephone +46 31 772 1000

Typeset in L<sup>A</sup>T<sub>E</sub>X  
Gothenburg, Sweden 2015

Synthesis and Quality Control of Radiohalogenated PSMA Inhibitors  
for Targeted Therapy of Prostate Cancer  
TIERRA DUFFIELD  
Department of Nuclear Engineering  
Chalmers University of Technology

## Abstract

Radioimmunotherapy and the development of radiopharmaceuticals is growing in its diversity and applications as method for treating disseminated tumors, with occult or manifest metastasis, at various locations of the body.  $^{211}\text{At}$  and  $^{125}\text{I}$  are two compounds that have desirable traits for radioimmunotherapy.  $^{211}\text{At}$  has a half-life of 7.2 hours and both modes of decay result in an  $\alpha$ -particle. It is also desirable because it decays to stable  $^{207}\text{Pb}$ .  $^{125}\text{I}$  has a half-life of 57.4 days and emits auger electrons, which are extremely cytotoxic, and decays to stable  $^{125}\text{Te}$ .

Prostate specific membrane antigen (PSMA) is 100 kDa type II trans-membrane protein highly expressed in prostate cancer and the vasculature of most solid tumors. This makes it the target for a number of therapeutic strategies. A molecule has been developed, ATE-P-1095 that when halogenated binds with high exclusivity to PSMA. The purpose of this thesis was to maximize the synthesis and establish the quality control for the radiohalogenation of ATE-P-1095 with  $^{125}\text{I}$  and  $^{211}\text{At}$ .

This was done by the electrophilic substitution of the trimethyl-tin group on the ATE-P-1095 for  $^{125}\text{I}$  or  $^{211}\text{At}$ . The components of the reaction were varied to maximize the output and quality of the synthesis. The parameters used to establish the quality control were radiochemical yield (RCY), radiochemical purity (RCP) and specific activity (SA). RCY greater than 95% were obtained for  $^{125}\text{I}$  with a maximum SA of  $918.18 \pm 36.24 \text{ MBq/mg}$  and 99% RCP. The  $^{211}\text{At}$  synthesis had a maximum RCY of 85.6% with a SA of  $230.16 \pm \text{ MBq/mg}$  and a 99% RCP.

After the quality control was maximized cell binding studies were done for  $^{125}\text{I}$ -MIP-1095 and  $^{211}\text{At}$ -MAP-1095 to the LNCaP cell line. The cell binding experiments showed  $B/T$  values between 6% -33% for both [ $^{125}\text{I}$ ]-MIP-1095 and [ $^{211}\text{At}$ ]-MAP-1095. For both molecules the  $B/T$  went up as the concentration decreased. A further decrease in concentration is likely to yield higher  $B/T$  or an increase in the number of LNCaP cells.

Keywords: targeted therapy, radioimmunotherapy, prostate cancer, PSMA, radiohalogenation, astatine-211, iodine-125.



## Acknowledgements

My master's thesis work at Sahlgrenska has been a great learning experience and I would like to give the sincerest thanks to all those involved in making it happen:

Emma Aneheim for being a great supervisor during the radiopharmaceutical course, introducing me to this topic and all of your help and guidance once I started working.

My supervisor Sture Lindegren for being a great teacher, showing me around the lab and introducing me to the different types of equipment, and always having time to answer questions. To my co-supervisor, Tom Bäck, who's interesting project was a joy to be a part of.

To Anna Gustafsson, whom I shared an office with, for always being willing to help and answer questions and to Helena Kahu for providing the cells used in my experiments.

I would like to thank all the people in the Department of Radiation Physics at Sahlgrenska for making it such an enjoyable place to work.

I would like to give the warmest thanks to my friends and family: Michelle Duffield who has been my ultimate guiding force and has provided the foundation I have built my life on, Tom Duffield's constant support has acted as the cornerstone of my growth and allowed me the freedom to take risks, and Georgi Dungarov for his perspective, friendship and never-ending patience.

Tierra Duffield, Gothenburg, May 2015



# Contents

<b>List of Figures</b>	<b>x</b>
<b>List of Tables</b>	<b>xiii</b>
<b>1 Introduction</b>	<b>1</b>
1.1 Background . . . . .	1
1.2 Prostate Cancer . . . . .	1
1.3 Targeted Therapy . . . . .	2
1.4 Radionuclides . . . . .	4
1.4.1 Iodine . . . . .	4
1.4.2 Astatine . . . . .	5
1.5 Prostate Specific Membrane Antigen . . . . .	5
1.6 Aims of this Thesis . . . . .	6
<b>2 Methods</b>	<b>7</b>
2.1 Reference Compound . . . . .	7
2.2 Radiohalogenation . . . . .	7
2.2.1 Iodine-125 . . . . .	8
2.2.2 Astatine-211 . . . . .	9
2.3 Cell Binding . . . . .	10
2.4 Optimization and Quality Control . . . . .	11
2.4.1 Specific Activity . . . . .	11
2.4.2 Radiochemical Yield . . . . .	12
2.4.3 Radiochemical Purity . . . . .	12
<b>3 Results</b>	<b>13</b>
3.1 Reference Compound . . . . .	13
3.2 Iodine . . . . .	14
3.2.1 Radiochemical Purity . . . . .	15
3.2.2 NIS . . . . .	15
3.2.3 Initial Activity . . . . .	16
3.2.4 Oxidant . . . . .	17
3.2.5 Column Flow Rate . . . . .	18
3.2.6 Molecular Degradation . . . . .	19
3.3 Astatine . . . . .	20
3.3.1 Radiochemical Purity . . . . .	20
3.3.2 NIS . . . . .	20

3.3.3	Initial amount of $^{211}\text{At}$ . . . . .	23
3.4	Comparison between $^{211}\text{At}$ and $^{125}\text{I}$ . . . . .	24
3.5	Cell Binding . . . . .	26
3.6	Comparison with K. Maresca . . . . .	29
<b>4</b>	<b>Conclusion</b>	<b>31</b>
	<b>Bibliography</b>	<b>33</b>
<b>A</b>	<b>Iodination Protocol</b>	<b>I</b>
<b>B</b>	<b>Astatination Protocol</b>	<b>III</b>
<b>C</b>	<b>Radio-HPLC Spectra</b>	<b>V</b>
<b>D</b>	<b>Cell Binding</b>	<b>XXI</b>
<b>E</b>	<b>Error Propagation</b>	<b>XXIII</b>

# List of Figures

1.1	The relationship between LET and RBE [5] . . . . .	3
1.2	Three types of radiation induced DNA damage . . . . .	4
1.3	Simplified decay scheme for $^{211}\text{At}$ . . . . .	5
2.1	Electrophilic substitution reaction for the addition of iodine or astatine to to form MIP-1095/MAP-1095 . . . . .	8
3.1	HPLC spectra for a nonradioactive I-MIP-1095 . . . . .	13
3.2	HPLC spectra for a nonradioactive I-MIP-1095 before and after passing through a Bond Elute Plexa column . . . . .	14
3.3	A radio-HPLC spectra comparing the influence of excess NIS solution, high radioactivity and low oxidant concentration on the RCY of [ $^{125}\text{I}$ ]-MIP-1095 . . . . .	15
3.4	A comparative plot showing the influence of excess NIS on the radiochemical yield and specific activity of [ $^{125}\text{I}$ ]-MIP-1095 . . . . .	16
3.5	A comparative plot showing the influence of the added activity on the radiochemical yield and the specific activity of [ $^{125}\text{I}$ ]-MIP-1095 . . . . .	17
3.6	A surface contour plot showing the influence of excess NIS and the initial activity on the radiochemical yield and specific activity of [ $^{125}\text{I}$ ]-MIP-1095 . . . . .	17
3.7	A comparative plot showing the influence of the amount of oxidant, chloramine-T, on the radiochemical yield and the specific activity of [ $^{125}\text{I}$ ]-MIP-1095 . . . . .	18
3.8	A comparative plot showing the influence of the column flow rate on the radiochemical yield [ $^{125}\text{I}$ ]-MIP-1095 . . . . .	19
3.9	A comparative plot showing differences between [ $^{125}\text{I}$ ]-MIP-1095 directly after synthesis and after 3 weeks. . . . .	19
3.10	A radio-HPLC spectra comparing the influence of excess NIS solution, high radioactivity on the RCP of [ $^{211}\text{At}$ ]-MAP-1095 . . . . .	21
3.11	A comparative plot showing the influence of excess NIS on the radiochemical yield and specific activity of [ $^{211}\text{At}$ ]-MAP-1095 with a starting molar amount of 43 nmoles MAP-1095 . . . . .	22
3.12	A comparative plot showing the influence of excess NIS on the radiochemical yield and specific activity of [ $^{211}\text{At}$ ]-MAP-1095 with a starting molar amount of 54 nmoles ATE-P-1095 . . . . .	23

---

3.13	A comparative plot showing the influence of the molar amount of $^{211}\text{At}$ on the radiochemical yield and specific activity of [ $^{211}\text{At}$ ]-MAP-1095 . . . . .	24
3.14	A comparative plot showing the differences in the HPLC spectrum between [ $^{211}\text{At}$ ]-MAP-1095 and activity of [ $^{125}\text{I}$ ]-MIP-1095 . . . . .	25
3.15	A comparative plot showing the differences in the radiation spectrum between $^{211}\text{At}$ -MAP-1095 and activity of [ $^{125}\text{I}$ ]-MAP-1095 . . . . .	25
3.16	A comparative plot showing the influence of the amount of $^{211}\text{At}$ on the $B/T$ of [ $^{211}\text{At}$ ]-MAP-1095 to LNCaP cells. . . . .	27
3.17	A comparative plot showing the influence of the temperature on the $B/T$ of $^{125}\text{I}$ -MAP-1095 to LNCaP cells. . . . .	28
3.18	A comparative plot showing the influence of the amount of $^{125}\text{I}$ on the $B/T$ of [ $^{125}\text{I}$ ]-MIP-1095 to LNCaP cells. . . . .	28
C.1	HPLC spectrum for product A, conducted on 2015/02/02, [ $^{125}\text{I}$ ]-MIP-1095 . . . . .	V
C.2	HPLC spectrum for product B, conducted on 2015/02/02, [ $^{125}\text{I}$ ]-MIP-1095 . . . . .	VI
C.3	HPLC spectrum for sample A, conducted on 2015/02/02, [ $^{125}\text{I}$ ]-MIP-1095 . . . . .	VI
C.4	HPLC spectrum for sample B, conducted on 2015/02/02, [ $^{125}\text{I}$ ]-MIP-1095 . . . . .	VII
C.5	Radio-HPLC spectrum for the product, conducted on 2015/02/11, [ $^{211}\text{At}$ ]-MAP-1095 . . . . .	VII
C.6	Radio-HPLC spectrum for the product 1 immediately after synthesis, conducted on 2015/02/18, [ $^{211}\text{At}$ ]-MAP-1095 . . . . .	VIII
C.7	Radio-HPLC spectrum for the product 2 immediately after synthesis, conducted on 2015/02/18, [ $^{211}\text{At}$ ]-MAP-1095 . . . . .	VIII
C.8	Radio-HPLC spectrum for the product 1 three hours after synthesis, conducted on 2015/02/18, [ $^{211}\text{At}$ ]-MAP-1095 . . . . .	IX
C.9	Radio-HPLC spectrum for product 1 immediately after synthesis, conducted on 2015/03/04, [ $^{211}\text{At}$ ]-MAP-1095 . . . . .	IX
C.10	Radio-HPLC spectrum for product 2 immediately after synthesis, conducted on 2015/03/04, [ $^{211}\text{At}$ ]-MAP-1095 . . . . .	X
C.11	HPLC spectrum for reference molecule before entering the column conducted on 2015/03/18, MIP-1095 . . . . .	X
C.12	HPLC spectrum for reference molecule before entering the column, a second verification, conducted on 2015/03/18, MIP-1095 . . . . .	XI
C.13	HPLC spectrum for reference molecule after entering the column conducted on 2015/03/18, MIP-1095 . . . . .	XI
C.14	Radio-HPLC spectrum for product 1 immediately after synthesis, conducted on 2015/03/18, [ $^{125}\text{I}$ ]-MIP-1095 . . . . .	XII
C.15	Radio-HPLC spectrum for sample 1 immediately after synthesis, conducted on 2015/03/18, [ $^{125}\text{I}$ ]-MIP-1095 . . . . .	XII
C.16	Radio-HPLC spectrum for sample 2 immediately after synthesis, conducted on 2015/03/18, [ $^{125}\text{I}$ ]-MIP-1095 . . . . .	XIII

---

C.17 Radio-HPLC spectrum for product 1 immediately after synthesis, conducted on 2015/03/25, [ $^{211}\text{At}$ ]-MAP-1095 . . . . .	XIII
C.18 Radio-HPLC spectrum for product 2 immediately after synthesis, conducted on 2015/03/25, [ $^{211}\text{At}$ ]-MAP-1095 . . . . .	XIV
C.19 Radio-HPLC spectrum for sample 1 immediately after synthesis, conducted on 2015/03/25, [ $^{211}\text{At}$ ]-MAP-1095 . . . . .	XIV
C.20 Radio-HPLC spectrum for sample 2 immediately after synthesis, conducted on 2015/03/25, [ $^{211}\text{At}$ ]-MAP-1095 . . . . .	XV
C.21 Radio-HPLC spectrum for product 1 immediately after synthesis, conducted on 2015/03/27, [ $^{125}\text{I}$ ]-MIP-1095 . . . . .	XV
C.22 Radio-HPLC spectrum for product 2 immediately after synthesis, conducted on 2015/03/27, [ $^{125}\text{I}$ ]-MIP-1095 . . . . .	XVI
C.23 Radio-HPLC spectrum for product 1 immediately after synthesis, conducted on 2015/04/01, [ $^{125}\text{I}$ ]-MIP-1095 . . . . .	XVI
C.24 Radio-HPLC spectrum for product 2 immediately after synthesis, conducted on 2015/04/01, [ $^{125}\text{I}$ ]-MIP-1095 . . . . .	XVII
C.25 Radio-HPLC spectrum for product 3 immediately after synthesis, conducted on 2015/04/01, [ $^{125}\text{I}$ ]-MIP-1095 . . . . .	XVII
C.26 Radio-HPLC spectrum for product 1 three weeks after synthesis, conducted on 2015/04/01, [ $^{125}\text{I}$ ]-MIP-1095 . . . . .	XVIII
C.27 Radio-HPLC spectrum for product 2 three weeks after synthesis, conducted on 2015/04/01, [ $^{125}\text{I}$ ]-MIP-1095 . . . . .	XVIII
C.28 Radio-HPLC spectrum for product 1 immediately after synthesis, conducted on 2015/04/08, [ $^{211}\text{At}$ ]-MAP-1095 . . . . .	XIX
C.29 Radio-HPLC spectrum for product 1 immediately after synthesis, conducted on 2015/04/08, [ $^{211}\text{At}$ ]-MAP-1095 . . . . .	XIX



# List of Tables

2.1	Summary of varied parameters for the [ $^{125}\text{I}$ ]-MIP-1095 labeling experiments * stock concentration of 7.14 <i>mg/ml</i> . . . . .	8
2.2	Summary of varied parameters for the [ $^{211}\text{At}$ ]-MIP-1095 labeling experiments . . . . .	10
3.1	Summary of all I-125 labeling experiments . . . . .	14
3.2	Summary of all $^{211}\text{At}$ labeling experiments . . . . .	20
3.3	Summary of cell binding labeling experiments for $^{211}\text{At}$ and $^{125}\text{I}$ at room temperature . . . . .	26
3.4	Summary of cell binding labeling experiments for $^{125}\text{I}$ at room temperature and in an ice bath . . . . .	27
3.5	Summary of calculations for the ratio of the number of $^{125}\text{I}$ -MIP-1095 and $^{211}\text{At}$ -MAP-1095 molecules to the number of LNCaP cells. . . . .	29
3.6	Summary of calculations for the ratio of the number of $^{125}\text{I}$ -MIP-1095 molecules to the number of LNCaP cells. . . . .	29
D.1	Comprehensive list of At-211 and I-125 cell binding experiments at room temperature . . . . .	XXI
D.2	Comprehensive list of I-125 cell binding experiments in an ice bath and at room temperature . . . . .	XXI
E.1	A summary of the uncertainties (unc), relative uncertainty (rel. unc.) and the range (U) in the specific activity (SA) calculations. . . . .	XXIV



# 1

## Introduction

### 1.1 Background

There are a variety of cancer treatments available today, ranging from surgery, chemotherapy and external radiation therapy. A form of therapy that is growing in its diversity and applications is targeted radiation therapy or radioimmunotherapy (RIT). The premise is that an alpha or beta-emitting molecule, chosen based on the size and density of the tumor, is attached to a molecule or antibody that selectively targets the tumor or antigen specifically expressed on the surface of the tumor cell. This can be a benefit for disseminated tumors with occult or manifest metastasis at various locations in the body. The established treatment is currently systemic chemotherapy, which is often toxic and can lead to chemotherapy-resistant cells. The main objective of this thesis is to optimize the synthesis and subsequent quality control of the radiolabeling of a molecule that targets prostate specific membrane antigen (PSMA), which is overly expressed on the surface of prostate cancer cells. This may provide an additional component in the treatment of disseminated prostate cancer.

### 1.2 Prostate Cancer

An estimated 220,800 men will be diagnosed with prostate cancer in United States in 2015, making it one of the most diagnosed types of cancer in men. Approximately 27,540 deaths will result from prostate cancer in the United States. It is the second leading cause of cancer death in men [1]. The latency period for radiation induced cancer is considered to be 5–7 years for leukemia, and for solid tumours at least 10 years [2]. Due to the fact that men are living much longer with the disease, clinical decision are important for selecting a treatment. These long-term survivors experience a significant incidence of chronic health problems after their treatment, including second primary cancer [3]. A second cancer is defined as a histologically distinct cancer that develops after the first cancer [4]. The ability to minimize relapse, maximize the efficiency of treatments while eradicating cancer cells has become more challenging.

## 1.3 Targeted Therapy

Targeted therapy has some distinct advantages over traditional radiation therapy. Traditional external radiation therapy, via gamma radiation, can lead to high doses to healthy tissue. The energy from the incident radiation is deposited primarily at the surface of the body. As the gamma rays pass through the body energy is attenuated in the healthy tissue and the gamma ray loses energy depending on the distance of travel and the density of the material. Unless the tumor is on the surface of the body the radiation absorbed in the tumor is usually less than, or equal to, that of the surrounding healthy tissue. This is why doses need to be fractionated and irradiation occurs from multiple locations. Targeted radiation therapy is an internal therapy that has the potential to greatly increase the therapeutic window by increasing the ratio of dose to tumor tissue versus healthy tissue. Critical organs such as the liver, thyroid and kidneys are still important to take into account as accumulation of the molecule often occurs in these organs.

The main types of radiation used in targeted therapy are beta emitting radionuclides and alpha emitting radionuclides. Radiation type is selected based on the size of the tumor: beta particles are used for tumors on the mm - cm scale, while alpha is used for mm scale tumors and auger electrons are used for micrometastasis. This allows for very concentrated dose due to the high linear energy transfer (LET) of these types of radiation. A high LET means that the energy released from the radiation is done so in a more concentrated volume than something with low LET, like gamma rays or X-rays. Since the energy is concentrated it leads to a localized dose to the tumor cell, and a reduced dose to healthy tissue. An important factor to consider in both internal and external radiation therapy is the oxygen enhancement ratio (OER). Gamma radiation causes most of its damage by indirect effects, such as the hydrolysis of water in the body. These indirect effects need oxygen, which cause it to be a limiting factor in hypoxic tumors. Alpha radiation is not subject to the same problem as its interactions with DNA are primarily through direct effects.

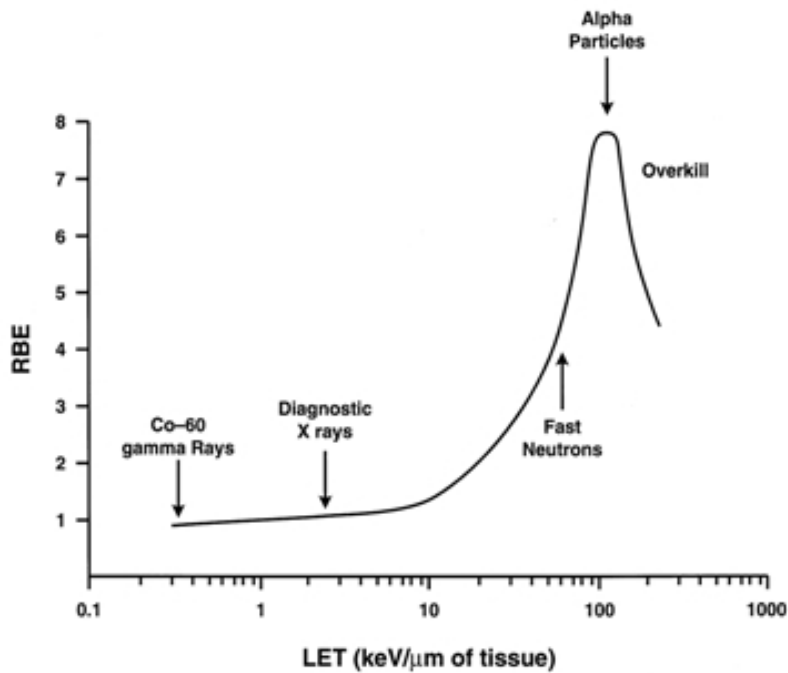


**Figure 1.1:** The relationship between LET and RBE [5]

The short range of very energetic alpha emissions in tissue means that a large fraction of that radiative energy goes into the targeted cancer cells, once a carrier, such as a monoclonal antibody, has taken the alpha-emitting radionuclide to the tumor. Alpha particles have an ideal radiobiological effect (RBE), shown in figure 1.1 due to the ability to cause double-strand breaks in the DNA. There are three main types of DNA damage, shown in figure 1.2: single-strand breaks, double-strand breaks nonconsecutive, and double-strand breaks consecutive. Single-strand breaks are easy for the body to repair, as are nonconsecutive double-strand breaks since they are treated as 2 single-strand breaks. Consecutive double-strand breaks are very difficult to repair and the cell often is not able to repair it or it is mis-repaired as it involves complete sheering of the DNA. This can lead to a mutation or cell death. This is more likely to happen during different stages of the cell cycle, meaning that cells that divide frequently are more susceptible to radiation. Cancer cells are rapidly dividing cells and are thus very susceptible to the effects of radiation.

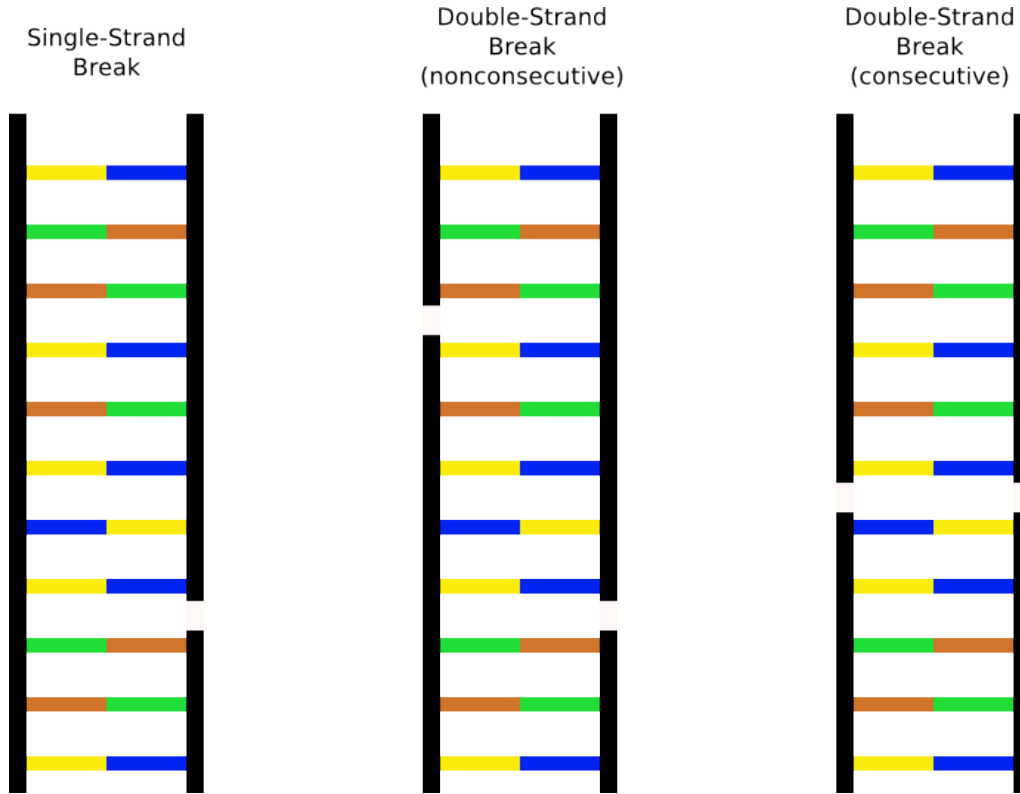


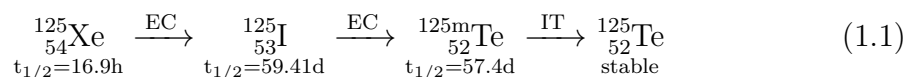
**Figure 1.2:** Three types of radiation induced DNA damage

There are multifaceted reasons RIT for solid tumor malignancies has been slower to develop. Reasons for this are lack of specific antigens and antibodies optimized for RIT, difficulties in linking radionuclides, shortfalls in readily available radionuclides and the difficulty in clinical use[6]. Another issue with targeted therapy is attaching the radionuclide to an antibody due to its large size and relatively long circulation times in the body. This leads to larger doses to healthy tissue. A variety of methods are being developed to combat this issue: one is a pre-targeting method where the antibody binds to the antigen expressed on the tumor cell and then the radionuclide attached to a linker is injected, which will bind to the antibody, another is to attach the radionuclide to antibody fragments or to a small molecule designed to bind exclusively to the specific antigen.

## 1.4 Radionuclides

### 1.4.1 Iodine

The half-life of  $^{125}\text{I}$  is 59.4 days, it is the second longest lived isotope of iodine. The biological half-life is 120-138 days for unbound iodine and an effective half-life of 42 days[7]. It is a radionuclide produced in a reactor through the bombardment of xenon gas. A simplified version of the  $^{125}\text{Xe}$  decay chain is shown in equation 1.1.



$^{125}\text{I}$  decays by electron capture, with a decay energy of 0.186 MeV, to the excited state of  $^{125}\text{Te}$ , which has a half-life of 57.4 days.  $^{125m}\text{Te}$  decays via isomeric transition to stable  $^{125}\text{Te}$  [8]. The Auger effect is when electron vacancies resulting from the internal conversion are filled by rearrangement of electrons in the outer shell until the valence shell is reached. Auger electrons are extremely cytotoxic and result in double-strand breaks if released in close proximity to the genome [9].

### 1.4.2 Astatine

$^{211}\text{At}$  decays by a double branch pathway, shown in figure 1.3. Each of the decay branches yield an  $\alpha$ -particle. The first branch (58.2%),  $^{211}\text{At}$  decays by electron capture to  $^{211}\text{Po}$ , which quickly decays to stable  $^{207}\text{Pb}$  via  $\alpha$ -decay. The second branch (41.8%) involves direct  $\alpha$ -particle emission to  $^{207}\text{Bi}$ .  $^{207}\text{Bi}$  undergoes electron capture to stable  $^{207}\text{Pb}$ . [8] The range of the  $\alpha$  particles in tissue is between 48 to 70  $\mu\text{m}$ .

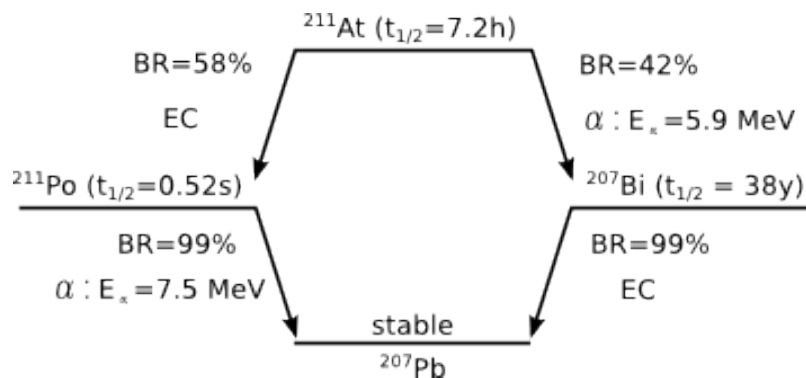


**Figure 1.3:** Simplified decay scheme for  $^{211}\text{At}$

The valence states of astatine are similar to those of iodine: -1, 0, +1, +3, +5 and +7. A special property of astatine is self-irradiation effects at high concentrations [10] and the high LET radiation may induce self-radiolysis and different oxidation states may occur simultaneously [10]. The radiotoxicity of  $^{211}\text{At}$  is classified as class II, or high radiotoxicity, together with  $^{125}\text{I}$  [11].

## 1.5 Prostate Specific Membrane Antigen

An antibody generator, abbreviated antigen (Ag), is a structural substance which serves as a target for the receptors of an adaptive immune response [12]. PSMA is a 100 kDa type II transmembrane protein that is highly expressed in prostate cancer and the vasculature of most solid tumors, making it the current target of a number of diagnostic and therapeutic strategies [13]. The role PSMA plays in prostate cancer is still unknown. The higher expressing tumors have been associated with faster progression and a great percentage of patients suffering from relapse [14].

Radiolabeled monoclonal antibodies that bind to the extracellular domain of PSMA were shown to accumulate in PSMA-positive prostate tumors in animals [15]. They hold promise for tumor detection and therapy, but clinical successes have been limited in large part because large molecules exhibit poor permeability in solid tumors and slow clearance from the circulation system. Low molecular weight compounds tend to have higher permeability into solid tumors and have more rapid tissue distribution and faster blood clearance [16]. A series of novel halogen-containing glutamate urea heterodimers based on glutamate-urea-lysine were designed and synthesized by Molecular Insight Pharmaceuticals, Inc. [17]. From these, a small molecule was identified, halogenated ATE-P-1095, that binds with high affinity to PSMA and accumulates in metastatic prostate cancer [17].

### 1.6 Aims of this Thesis

The main objective of this master thesis is to optimize the synthesis and subsequent quality control of the radiolabeling of a stannylated precursor abbreviated as ATE-P-1095. It can be subjected to destannylation, with  $^{125}\text{I}$  and the alpha emitter  $^{211}\text{At}$ . This PSMA targeting molecule MIP-1095/MAP-1095 labeled with a radioactive alpha emitter can be used for target alpha therapy, which may provide an additional component in the treatment of disseminated prostate cancer.

The first stage of the experimental plan is to develop a protocol to radiolabel the ATE-P-1095 with  $^{125}\text{I}$ . An initial protocol for synthesis with  $^{125}\text{I}$  and  $^{211}\text{At}$  was developed based on previous experiments with  $^{131}\text{I}$ . The necessary components for the synthesis are dissolving the ATE-P-1095 residue in an aqueous solution, adding an oxidizing agent and the radionuclide, incubation, and then adding a nonradioactive iodine compound to substitute the rest of the remaining trimethyl-tin groups on the MIP-1095/MAP-1095. Another compound needs to be added (such as trifluoric acid) to remove the protecting groups from the MIP-1095/MAP-1095, which were introduced to the molecule to obtain chemoselectivity. The solution is then diluted and ran through a column. The desired product sticks to the column and can be eluted with ethanol.

The solvents, iodination compounds and oxidizing agents are varied to obtain a high specific activity and radiochemical purity of the product to make it suitable for medical use. The product removed from the column is analyzed with radio-high performance liquid chromatography (HPLC) and a NaI well detector to establish the quality control of the molecule. Methods of separation such as thin layer chromatography (TLC) will be investigated. After the desired specific activity and radiochemical purity have been obtained the protocol for  $^{211}\text{At}$  was developed. Cell binding assays were done with both the iodinated and the astitinated compounds at room temperature and in ice to evaluate the binding efficiency of the molecule.

# 2

## Methods

### 2.1 Reference Compound

An initial experiment was conducted to establish the baseline HPLC spectra for the reference compound. The reference compound is a nonradioactive iodine labeled MIP-1095. 5 mg of MIP-1095 was dissolved in 1 ml of 95% ethanol. A 20  $\mu$ l sample was injected into the HPLC and eluted with a gradient of 95%, 0.1% TFA in MilliQ water and 5%, 0.1% TFA in ACN over 30 minutes.

Another experiment was conducted with the reference compound to establish if the I-MIP-1095 sticks to the Bond Elute Plexa column. A mass of 4.31 mg of I-MIP-1095 was added to 50  $\mu$ l 1% acetic acid (HAc) in methanol. This was diluted to 1 ml with 95% ethanol, split in a half and each volume was then diluted further to 1.2 ml. The first volume was analyzed directly on the HPLC. A volume of 25  $\mu$ l was injected into the HPLC and ran with the afore mentioned parameters. The second volume was put on a Bond Elute Plexa column activated with 3 ml of 20% ethanol in MilliQ water solution. The 1.2 ml of solution was passed through the column and collected. The product was analyzed on the HPLC using the same method as the initial sample. The peak area of the spectra were compared to establish the percentage of compound sticking to the column without further elution.

### 2.2 Radiohalogenation

A series of radiolabelings was done with  $^{125}\text{I}$  and  $^{211}\text{At}$ . The method of labeling used is the electrophilic substitution of the radioactive iodine or astatine for the trimethyl-tin group on the ATE-P-1095. Figure 2.1 illustrates the substitution reaction for a radioactive iodine species. Appendix A has the final labeling procedures for  $^{125}\text{I}$ -MIP-1095 and  $^{211}\text{At}$ -MAP-1095.

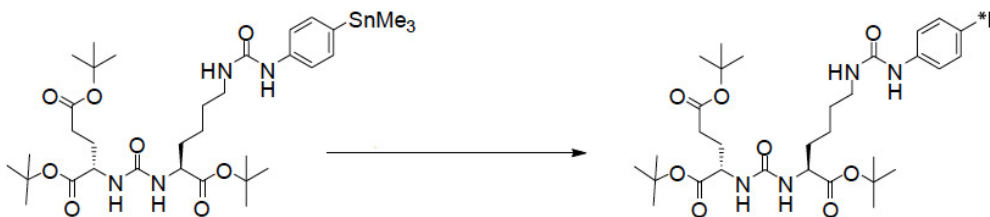


**Figure 2.1:** Electrophilic substitution reaction for the addition of iodine or astatine to to form MIP-1095/MAP-1095

### 2.2.1 Iodine-125

Two stock solutions of the ATE-P-1095 precursor molecule in chloroform were prepared with concentrations of  $8.87\text{ mg/ml}$  and  $7.14\text{ mg/ml}$ . The first step was to take  $5\ \mu\text{l}$  of stock solution and evaporate the chloroform under a stream of nitrogen. The residue was then dissolved in  $12\ \mu\text{l}$  of 1% acetic acid in methanol. Approximately 10 MBq to 30 MBq of  $\text{Na}[\text{}^{125}\text{I}]$  solution was added with  $1\ \mu\text{l}$  of 10 mg/ml chloramine-T in MilliQ water to oxidize the iodine. Next, a varying amount of excess of (1 mg/ml N-iodosuccinimide in 1% acetic acid in methanol) was added to substitute the remaining tin groups. It was then incubated with gentle agitation for 1 minute at room temperature. The solution was then resolved in 0.5 ml of neat trifluoroic acid to remove the tert-butyloxy carbonyl (BOC) protecting groups and incubated with gentle agitation for 15 minutes at room temperature. Table 2.1 is a summary of the varied experimental parameters for each experiment. During the incubation the Bond Elute Plexa columns were activated with 2-3 ml of 20% ethanol in MilliQ water.

Trial	Chloramine-T ( $\mu\text{l}$ )	[CT] (mg/ml)	ATE-P-1095 ( $\mu\text{l}$ )	Excess NIS ( $\mu\text{l}$ )	[NIS] (mg/ml)	I-125 (MBq)	Wash Volume
I-1	1	10.02	*5	3	1.29	3.09	3
I-2	1	9.99	5	0	0.99	5.5	3
I-3	1	9.99	5	1	0.99	6.5	3
I-4	1	10.07	5	5	1.00	12.1	3
I-5	1	10.07	5	10	1.00	12	3
I-6	1	9.96	5	3	1.00	38.3	2
I-7	1	5.28	5	3	1.00	9.6	2
I-8	2	9.96	5	3	1.00	11.6	3

**Table 2.1:** Summary of varied parameters for the [ $^{125}\text{I}$ ]-MIP-1095 labeling experiments

\* stock concentration of  $7.14\text{ mg/ml}$

The solution was diluted to a volume of 5 ml with MilliQ water and a  $50\ \mu\text{l}$  to 75

$\mu\text{l}$  sample was taken for radio-HPLC analysis. The reaction mixture was added to the Bond Elute Plexa column and washed with 2-3 ml of 20 % ethanol in MilliQ water. An air filled syringe was used to gently force the solution through the Bond Elute Plexa column. The product was then eluted with 500  $\mu\text{l}$  of 95 % ethanol. The activity of each of the components of the system, along with the samples, product and waste were recorded using a NaI well detector. Then the product was analyzed with a radio-HPLC as shown in Lindegren et al [18] to determine radiochemical purity. Briefly, A reference cell and an analytical cell were used to form a dual-flow cell constructed from two PEEK capillary coils to fit into the well of a NaI(Tl) detector. The flow is directed from the injector to the reference cell allowing on-line detection of the total amount of injected radioactivity prior to entering the HPLC column. The radioactivity eluted from the column is then detected in the analytical cell. This allows on-line quantification of the radioactivity passing through the system, as well as the standard HPLC spectrum. Both of the spectra were recorded using Max software.

### 2.2.2 Astatine-211

The astatine labeling follows a similar procedure to the iodine labeling due to the similarities in the chemistry of the two elements. The same stock solutions of ATE-P-1095 in chloroform were used. The same amount of stock solution, 5  $\mu\text{l}$ , was evaporated to dryness and dissolved in 12  $\mu\text{l}$  of 1 *mg/ml* NIS in 1 % acetic acid in methanol. The NIS solution was used, instead of just the 1 % acetic acid in methanol, to activate the  $^{211}\text{At}$  since chloramine-T would cause over-oxidization. The  $^{211}\text{At}$  was obtained by the steps outlined in Aneheim et al [19] and Lindegren et al [20].  $^{209}\text{Bi}$  targets are activated using 29 MeV alpha particles to create  $^{211}\text{At}$  at the PET and Cyclotron Unit at Copenhagen University Hospital, Denmark. The targets are comprised of a 20  $\mu\text{m}$  bismuth layer on an aluminum backing and sealed with 5  $\mu\text{m}$  aluminum layer. The thin aluminum layers are removed from the backing using a mechanical scraping device and the astatine is isolated from the bismuth by dry distillation at 670 °C in a tube furnace. The astatine is evaporated and the vapor is condensed in a chemically inert plastic capillary cooled to  $-79^\circ\text{C}$ . The condensed astatine is eluted from the capillary with chloroform and portioned into suitable vials and evaporated to dryness for further processing.

Astatine solution containing between 8 MBq- 20 MBq of activity was evaporated to dryness under a stream of nitrogen. The astatine residue is dissolved in the ATE-P-1095 solution. The solution was incubated for 1 minute with gentle agitation. Additional excess NIS is added, between 0-20  $\mu\text{l}$  to substitute the remaining tin groups and then incubated with gentle agitation for another minute. To remove the BOC-protection groups 0.5 *ml* of neat TFA was added and the solution was incubated for 15 minutes with gentle agitation. The Bond Elute Plexa columns were activated using 2-3 *ml* 20% ethanol in MilliQ water. Table 2.2 is a summary of the varied experimental parameters for each experiment.

Trial	ATE-P-1095 ( $\mu$ l)	Excess NIS ( $\mu$ l)	[NIS] (mg/ml)	At-211 (MBq)	Wash Volume
At-1	*5	20	1.15	11.72	3
At-2	*5	3	1.3	9.35	3
At-3	*5	20	1.3	9.24	3
At-4	5	0	0.85	11.95	3
At-5	5	3	0.85	8.71	3
At-6	5	5	0.9	13.6	2
At-7	5	10	0.9	12.72	2
At-8	5	3	1.09	14.07	3
At-9	5	3	1.09	26.2	3

**Table 2.2:** Summary of varied parameters for the [ $^{211}\text{At}$ ]-MIP-1095 labeling experiments

The solution is diluted to a volume of 5 mL with MilliQ water and a 50  $\mu$ l to 75  $\mu$ l sample was taken for HPLC analysis. The reaction mixture was added to the Bond Elut Plexa column, activated with 20 % ethanol in MilliQ water. The remaining liquid was purged from the column using an air filled syringe and the final product was eluted with 95 % ethanol and analyzed in the same was as the iodinated samples.

## 2.3 Cell Binding

A series of LNCaP cell binding assays were conducted with  $^{125}\text{I}$  and  $^{211}\text{At}$ . LNCaP cells are androgen-sensitive human prostate adenocarcinoma cells derived from the left supraclavicular lymph node metastasis [21]. The LNCaP cells were maintained in a RPMI-1640 medium and supplemented with 10 % fetal bovine serum. Three concentrations of  $^{211}\text{At}$ -MAP-1095 were prepared and one concentration of  $^{125}\text{I}$ -MIP-1095. The cells concentration was  $1 \times 10^7$  to  $2 \times 10^7$  cells in a 1.5 ml volume of growth medium. This was diluted to a final volume of 3 ml with growth medium. A stock solution was created with 7.6  $\mu$ l of astatine product (At-8) diluted in 600  $\mu$ l of growth medium. 100  $\mu$ l was diluted 5x and 100  $\mu$ l was further diluted to a final dilution of 25x. An initial solution of 4.1  $\mu$ l of iodine product (I-7) and 600  $\mu$ l of growth medium was used for the  $^{125}\text{I}$  trials. Each of the experiments were done in triplicate.

75  $\mu$ l of the prepared radioisotope solution was added to 200  $\mu$ l of cell solution. A Wizard 1480 automatic gamma counter was used to establish the amount of radioactivity added to the solution. Then, cells were agitated at room temperature for two hours. After incubation, the cells were centrifuged for 5 minutes at 30,000 rpm, the fluid was drained and the cells were washed. Since, the cells were not sticking properly to the walls of test tube phosphate buffered solution (PBS) was used instead of the growth medium to wash the cells. After adding 200  $\mu$ l PBS, the solution was agitated gently and then centrifuged for 5 minutes. The solution was removed from the cell pellet and the cells were measured in the gamma counter to

obtain the bound over total. shown in Equation 2.1.

$$B/T = \frac{A_{bound} - A_{tube}}{A_{tot}} \quad (2.1)$$

$A_{bound}$  is the activity bound to the cells, it is what is remaining after the washing and removal of excess fluid from the cells.  $A_{tot}$  is the initial activity added to each test tube.  $A_{tube}$  is the activity bound to the test tube. This was obtained by removing the cells from the test tubes of the highest concentrations experiments, washing them with PBS, and measuring the activity.

Another series of cell binding experiments were conducted to determine if the radioisotope was being internalized and the expelled from the cell. It was prepared similarly to the previous experiments. The cell concentration was  $1 \times 10^7$  per ml in a 4 ml volume. A stock solution of  $^{125}\text{I}$ -MIP-1095 was prepared from 10  $\mu\text{l}$  of product (I-7) in 1200 ml volume of growth medium. Then, 200  $\mu\text{l}$  of the stock solution was diluted with 800  $\mu\text{l}$  of growth medium. 100  $\mu\text{l}$  of stock solution and 300  $\mu\text{l}$  of cell solution was added to 6 vials, each of the experiments were done in triplicate, and the diluted solution was added into 6 more vials. The vials were counted to determine the initial radioactivity and then 3 vials with the stock concentration and 3 vials with the diluted concentration were kept at room temperature and the remaining 6 vials were placed in an ice bath. The cells were allowed incubate with gentle agitation for two hours. After the incubation the cells were centrifuged, washed and counted in the same way as the previous experiments.  $B/T$  values were obtained for each of the experiments.

## 2.4 Optimization and Quality Control

A series of calculations were done for each experiment to establish the quality control and improve optimization of the radiohalogenated MIP-1095/MAP-1095 synthesis.

### 2.4.1 Specific Activity

Equation 2.2 is the specific activity, or specific radioactivity (SA), which is defined as the decay rate  $A$  per unit amount of  $w$  of an element or compound [22]. In this case  $w$  is the amount of ATE-P-1095 added to the system. The SI unit for specific activity is  $Bq/kg$ .

$$SA = \frac{A}{w} \quad (2.2)$$

A high specific activity is important for medical purposed to minimize the amount of material that needs to be injected into the patient. Large doses are often needed for cancer treatment, in the  $GBq$  range, thus making it necessary to maximize specific activity.

### 2.4.2 Radiochemical Yield

Radiochemical yield is the yield of a radiochemical separation expressed as a fraction of the activity originally present ( $A_{int}$ ) [23]. The amount of desired product from the radiochemical separation is determined by the activity of the eluent from the column,  $A_{elute}$ .

$$RCY = \frac{A_{elute}}{A_{int}} \quad (2.3)$$

It is important to maximize the output of the experiment, or the RCY, due to  $^{211}\text{At}$  limited availability and to reduce costs and labor requirements for the synthesis.

### 2.4.3 Radiochemical Purity

Radionuclide impurities can arise from variations in beam energy during irradiation or low separation factors during chemical processing. Radionuclide identity and purity were checked with a NaI(Tl) detector. The radionuclide purity of  $^{125}\text{I}$  and  $^{211}\text{At}$  does not decrease with time based on the half-life since both radionuclides decay to stable elements. The chemical identity was checked by HPLC. The combination of radionuclide purity and chemical identity is referred to as radiochemical purity (RCP). For the purpose of these experiments the RCP is defined in Equation 2.4.

$$RCP = \frac{a_{product}}{a_{product} + a_{aop}} \quad (2.4)$$

Where  $a_{product}$  is the peak area of the desired product and  $a_{aop}$  is the peak area of all other peaks observed in the radio-HPLC spectrum.

# 3

## Results

### 3.1 Reference Compound

The reference I-MAP-1095 compound was used as a reference for the baseline HPLC spectrum. The compound has a very clear, solitary peak, at 15 minutes. This peak will shift to approximately 20 minutes if there are air bubbles in the system. Figure 3.1 illustrates a 20  $\mu\text{l}$  sample of nonradioactive I-MAP-1095.

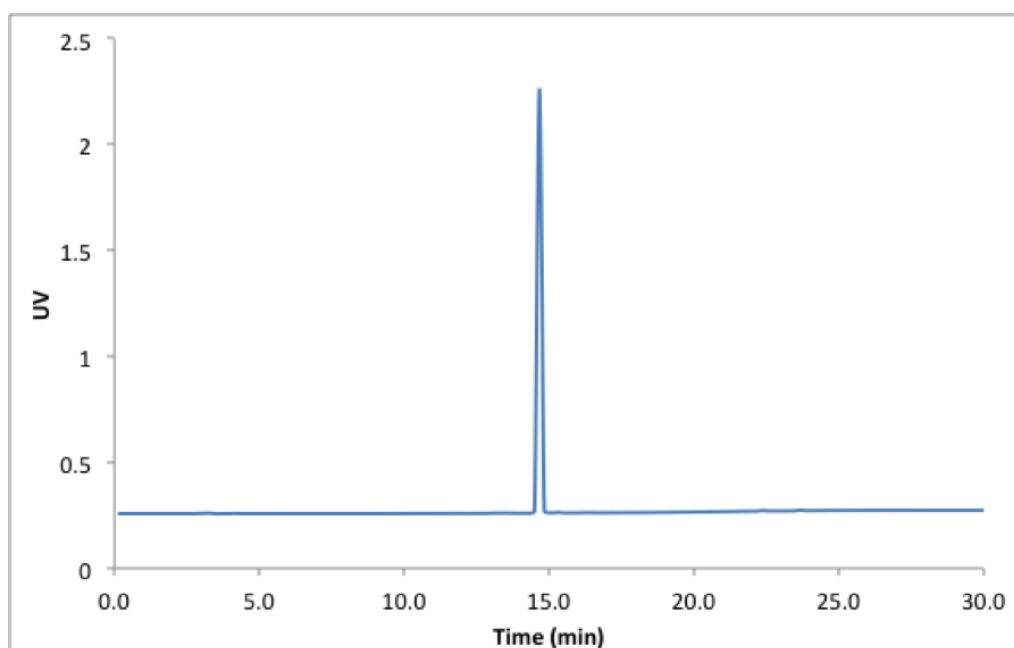


**Figure 3.1:** HPLC spectra for a nonradioactive I-MIP-1095

To establish the amount of labeled I-MIP-1095 that sticks to the column the reference compound was measured before and after passing through a Bond Elute Plexa column, shown in Figure 3.2. The peak area for each of curves was evaluated and compared to determine the amount of I-MIP-1095 removed from the column. The ratio of the peak area shows that only 54% of the I-MIP-1095 was recovered from the column. This could pose a problem for the recovery of the radiolabeled I-MIP-1095, but is likely due to a heterogeneous sample split. The shifting of the peak is caused by small bubbles trapped in the column.

### 3. Results

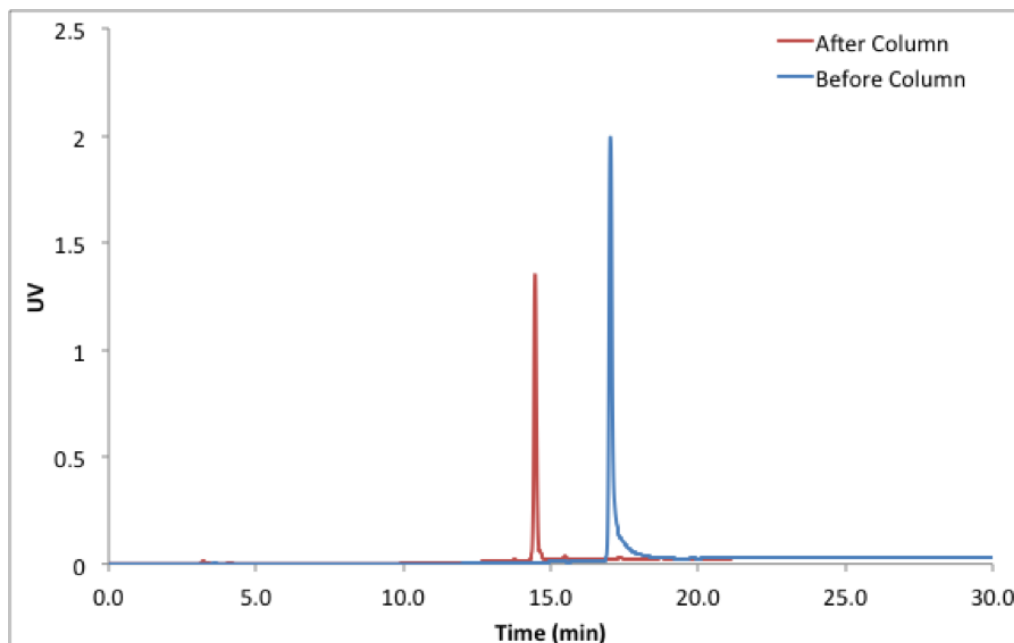


**Figure 3.2:** HPLC spectra for a nonradioactive I-MIP-1095 before and after passing through a Bond Elute Plexa column

## 3.2 Iodine

Since  $^{125}\text{I}$  was readily available, it was used first to optimize the protocol. A variety of experiments were conducted to show how the specific activity, radiochemical yield and the radiochemical purity were influenced by the amount of oxidizing agent for the  $^{125}\text{I}$ , the amount of  $\text{Na}^{125}\text{I}$  added, and the amount of excess  $\text{NIS}$  added. Table 3.1 is a summary of all the results of the  $^{125}\text{I}$  labeling experiments.

**Table 3.1:** Summary of all I-125 labeling experiments

Date	Trial	ATE-P-1095 (nmol)	CT (nmol)	NIS (nmol)	I-125 (nmol)	RCY	SA (MBq/mg)	Wash Volume (ml)
20150202	I-1	43	44	17	0.038	0.7	66.26±2.38	3
20150319	I-2	54	44	0	0.068	1	138.57±5.46	2
20150319	I-3	54	44	4.4	0.08	1	177.85±7.02	2
20150327	I-4	54	44	22	0.149	1	297.65±11.74	3
20150327	I-5	54	44	44	0.148	1	316.17±12.47	3
20150401	I-6	54	44	13	0.471	0.97	918.87±36.24	3
20150401	I-7	54	23	13	0.118	0.97	229.72±9.06	3
20150401	I-8	54	87.5	13	0.143	0.95	271.71±10.72	3

### 3.2.1 Radiochemical Purity

During experimentation three main parameters were established for each trial: radiochemical yield, specific activity and radiochemical purity. While the RCY and RCP were influenced by varying the amount of oxidizing agent, excess NIS solution and the initial activity, the RCP was largely unaffected. Figure 3.3 is a comparison plot between Trial I-5 (large amount of excess NIS solution), Trial I-6 (highest initial activity) and Trial I-7 (reduced chloramine-T concentration). The only variation in the plots comes with the activity of the sample, largely influenced by the injection volume into the column.

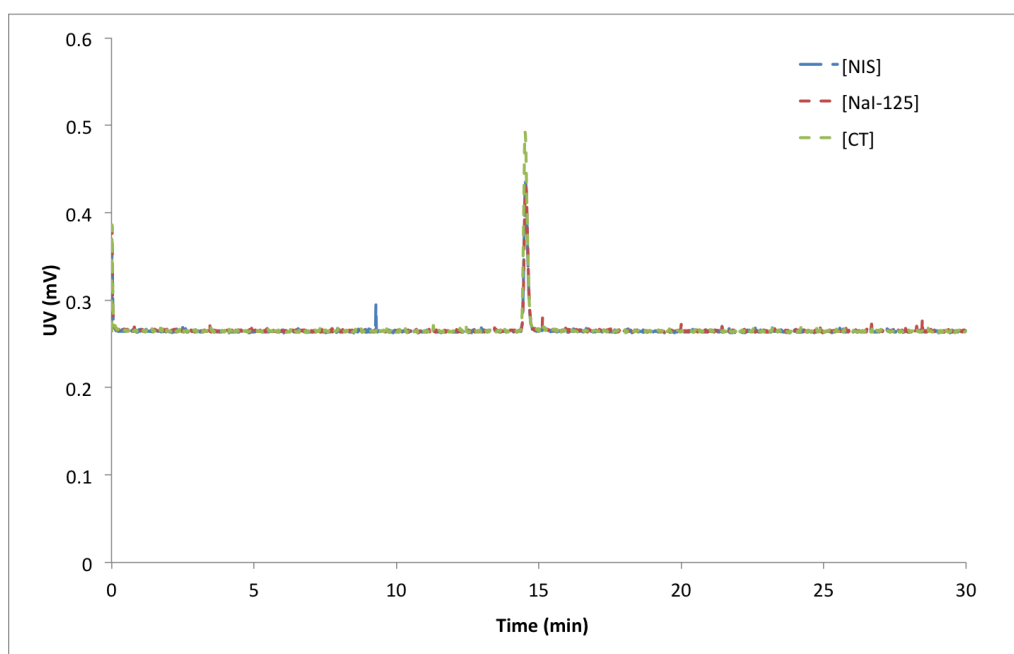


**Figure 3.3:** A radio-HPLC spectra comparing the influence of excess NIS solution, high radioactivity and low oxidant concentration on the RCY of [ $^{125}\text{I}$ ]-MIP-1095

### 3.2.2 NIS

The first thing varied was the amount of excess *NIS* used to substitute the remaining tin groups. A range of values between  $0\ \mu\text{l}$  and  $22\ \mu\text{l}$  were used in the experiments, which has been converted to the molar amount. Figure 3.4 shows the correlation between the amount of excess *NIS* and the radiochemical yield obtained from the experiment. The amount of excess *NIS* was not found to have a substantial influence on the RCY. There is a deviation from the 99% radiochemical purity in the first experiment, an *NIS* amount of 17 nmol. This is most likely due to an inadequate flow rate through the column due to a poor connection between the air-filled syringe and the column.

An upward trend is observed for the amount of excess *NIS* added and the specific activity obtained. A 10x increase in the amount of excess *NIS* shows an increased specific activity of 1.78x. The correlation between the amount of excess *NIS* and

### 3. Results

the specific activity is small, and is more likely due to the inadvertent increase in the initial amount of  $Na^{125}I$ .

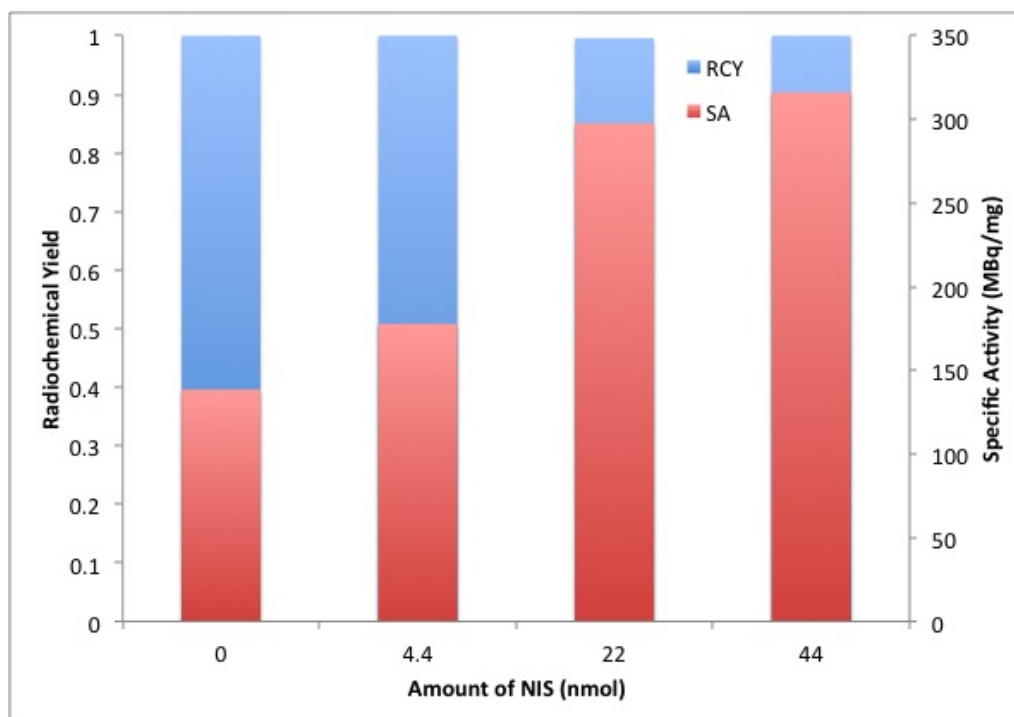


**Figure 3.4:** A comparative plot showing the influence of excess NIS on the radiochemical yield and specific activity of  $[^{125}I]$ -MIP-1095

#### 3.2.3 Initial Activity

The amount of radioactivity was varied in each experiment, both intentionally and unintentionally. A volume of  $3 \mu l$  varied between 0.08 nmol and 0.249 nmol. The activity was used to calculate the molar amount of  $^{125}I$ . In figure 3.5 a doubling of the initial activity results in almost a doubling of the specific activity. Then, an initial volume of  $6 \mu l$  was added, which resulted in 5x increase from the lower values.

There does not appear to be any correlation between the amount of initial  $^{125}I$  and the radiochemical yield at these small volumes. There is a slight decrease from  $>0.99$  to 0.97 observed during the experiments. This is most likely due to material attenuation seen in the iodine experiments. The reaction vial was a glass tube, while the product was collected in a plastic Eppendorf tube initially. After it became clear that there was some material attenuation observed in the measurements, the samples and products were collected in the glass vials.

A surface contour plot illustrates the dependence of specific activity on the amount of excess  $NIS$  and the initial amount of  $^{125}I$ , shown in Figure 3.6. The experiments with the highest specific activity were mostly dependent on the initial amount of

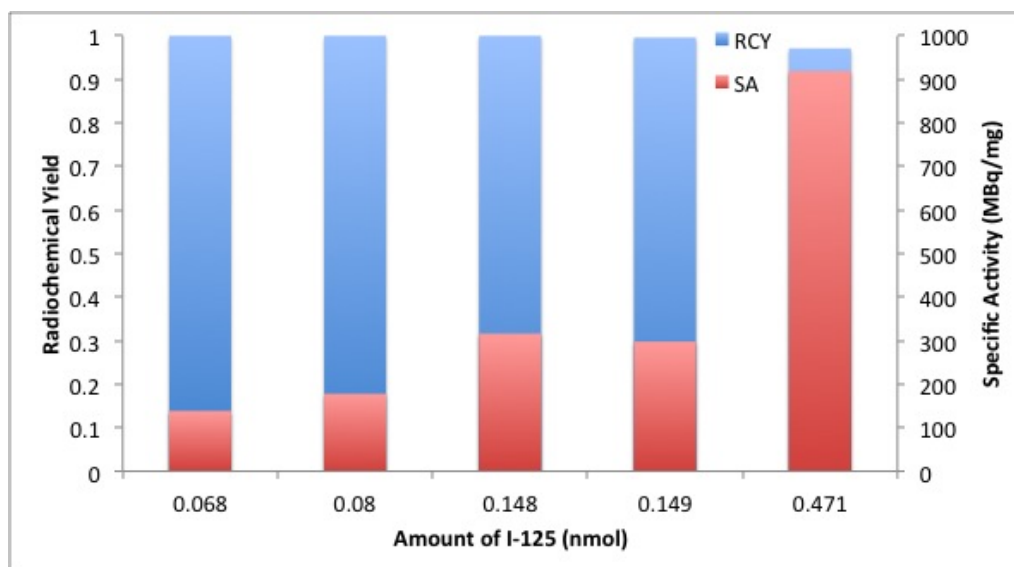


**Figure 3.5:** A comparative plot showing the influence of the added activity on the radiochemical yield and the specific activity of [ $^{125}\text{I}$ ]-MIP-1095

$^{125}\text{I}$ , but there does appear to be a range of NIS solution amounts where it is enough to substitute all remaining methyl-tin groups on the molecule and not be too much where it will be competitive with the  $^{125}\text{I}$ .

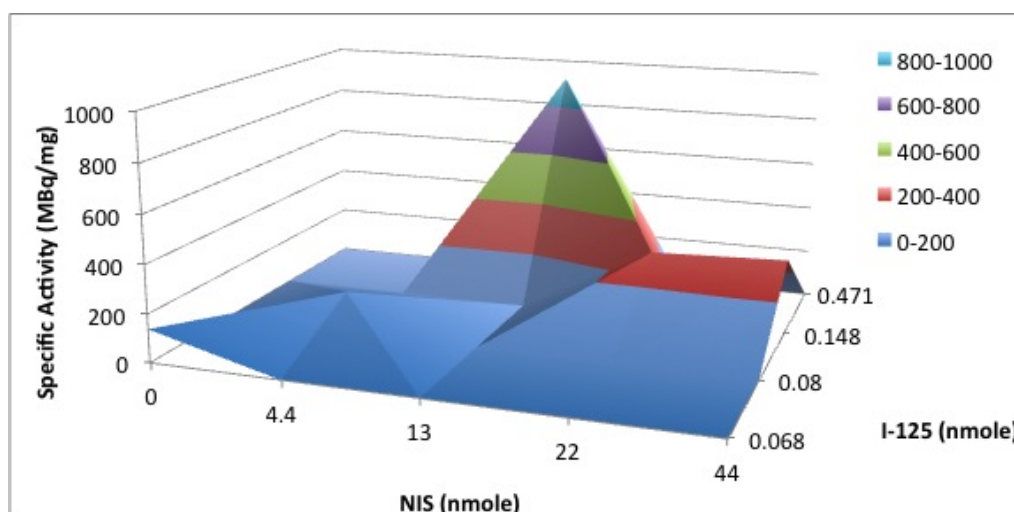


**Figure 3.6:** A surface contour plot showing the influence of excess NIS and the initial activity on the radiochemical yield and specific activity of [ $^{125}\text{I}$ ]-MIP-1095

### 3.2.4 Oxidant

Chloramine-T was chosen as the oxidizing agent because the hypochlorite released from chloramine-T forms iodine monochloride ( $\text{ICl}$ ).  $\text{ICl}$  rapidly undergoes electrophilic substitution with activated aromatic rings and is widely used for the incor-

### 3. Results

poration of iodine to peptides and proteins. Figure 3.7, shows a peak radiochemical yield and specific activity at 44 nmoles of chloramine-T. Higher values caused over oxidation of the  $^{125}\text{I}$  while smaller amounts of chloramine-T were not adequate for proper oxidization of  $^{125}\text{I}$ . This volume corresponded to a  $1\ \mu\text{l}$  of  $10\ \text{mg/ml}$  chloramine-T in MilliQ water solution.

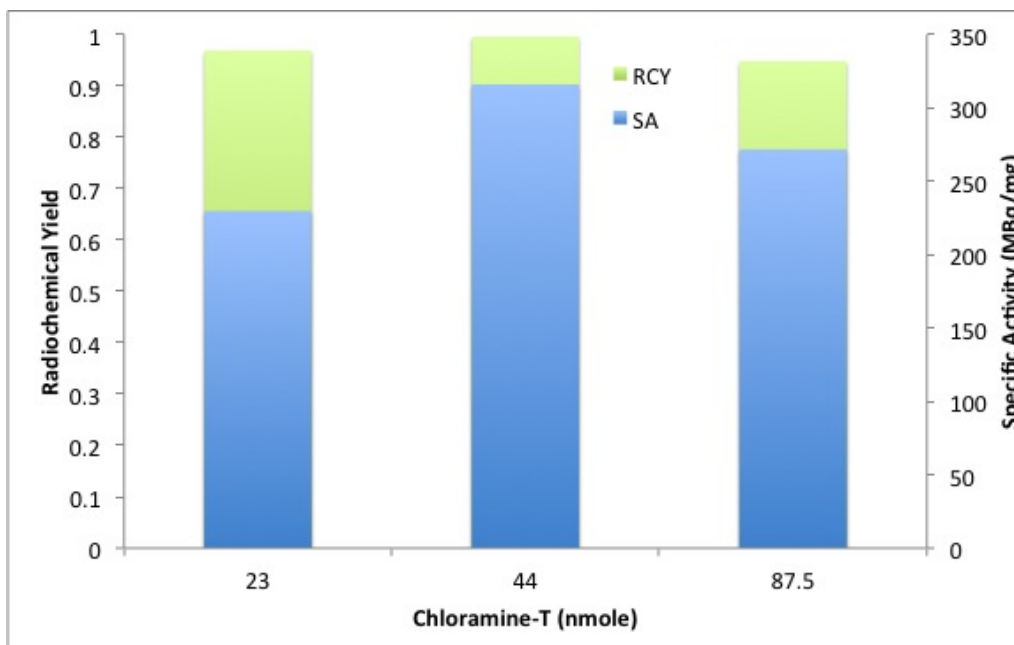


**Figure 3.7:** A comparative plot showing the influence of the amount of oxidant, chloramine-T, on the radiochemical yield and the specific activity of [ $^{125}\text{I}$ ]-MIP-1095

#### 3.2.5 Column Flow Rate

The column flow rate was found to have a large influence on the radiochemical yield. Agilent Technologies recommends a column flow rate of  $1\ \text{ml/min}$  for the Bond Elut Plexa column. Due to missing the proper adapters for the column, the first trial had a higher flow rate through the column, closer to  $2\ \text{ml/min}$ . This applies to the flow rate for putting the solution on the column, and the elution of the product from the column. Figure 3.8 illustrates the difference for radiochemical yield between the faster flow rate and the normal flow rate, below  $1\ \text{ml/min}$ . A radiochemical yield of 0.7 was obtained for the fast flow rate, while a value of 1.0 was obtained at the slower flow rates. At the faster flow rate slightly more radioactivity was observed in the wash, due to insufficient time for the [ $^{125}\text{I}$ ]-MIP-1095 to react with the column material, and less product was eluted because adequate solvation of the [ $^{125}\text{I}$ ]-MIP-1095 was not obtained at the higher flow rate.

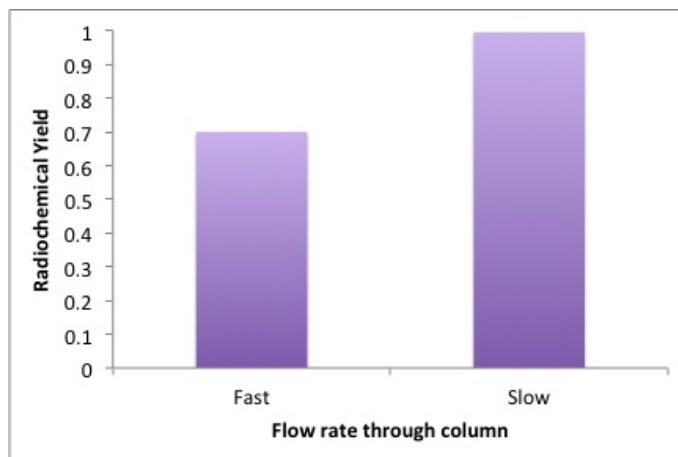


**Figure 3.8:** A comparative plot showing the influence of the column flow rate on the radiochemical yield [ $^{125}\text{I}$ ]-MIP-1095

### 3.2.6 Molecular Degradation

The experiment with the highest radioactivity (38.3 MBq) was measured after 3 weeks to see if any molecular degradation was occurring due to self-irradiation or other factors, shown in figure 3.9. The radio-HPLC spectra showed minimal differences between the sample analyzed right after the synthesis and the sample analyzed after 3 weeks. The sample is stable long after synthesis which when combined with the relatively long half-life of  $^{125}\text{I}$  is ideal for use in a medical facility. It can be stored and kept on-hand instead of having to wait for it to be produced.

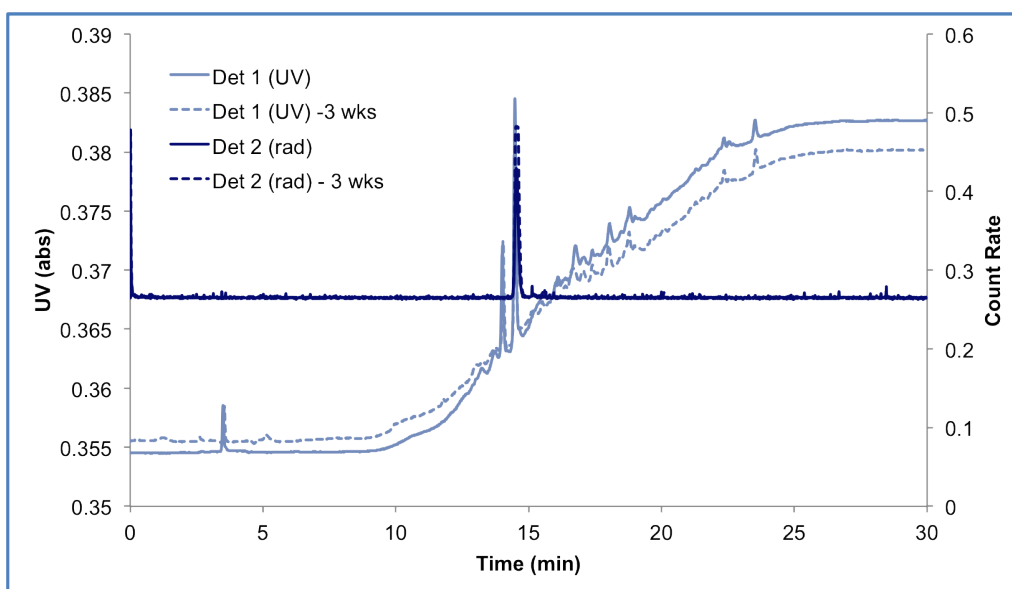


**Figure 3.9:** A comparative plot showing differences between [ $^{125}\text{I}$ ]-MIP-1095 directly after synthesis and after 3 weeks.

### 3.3 Astatine

Due to the method of production for  $^{211}\text{At}$  and its short half-life it was only available for experimentation every 2 weeks. After preliminary work with  $^{125}\text{I}$  experiments were conducted with  $^{211}\text{At}$ . An oxidizing agent was not used for  $^{211}\text{At}$  since it is prone to over-oxidizing. The amount of excess NIS was varied, the initial amount of stock ATE-P-1095 and the amount of  $^{211}\text{At}$  added.

**Table 3.2:** Summary of all  $^{211}\text{At}$  labeling experiments

Date	Trial	ATE-P-1095 (nmol)	NIS (nmol)	At-211 (nmol)	RCY	SA (MBq/mg)	Wash Volume (ml)
20150210	At-1	43	161	0.0007	0.35	113.88±4.09	3
20150217	At-2	43	86	0.0006	0.86	230.16±8.26	3
20150217	At-3	43	183	0.0006	0.2	50.47±1.81	3
20150303	At-4	54	45	0.0007	0.14	35.82±1.41	3
20150303	At-5	54	56	0.0006	0.61	116.84±4.61	3
20150325	At-6	54	75	0.0008	0.13	38.78±1.53	2
20150325	At-7	54	97	0.0008	0.13	35.57±1.40	2
20150408	At-8	54	72	0.0008	0.29	90.41±3.57	3
20150408	At-9	54	72	0.0016	0.09	54.10±2.13	3

#### 3.3.1 Radiochemical Purity

The comparison of the radiochemical purity for the  $^{211}\text{At}$ -MAP-1095 trials was not as direct as the [ $^{125}\text{I}$ ]-MIP-1095 trials. While only a single desired peak appeared at 15 minutes, the baseline was extremely noisy in the majority of the later trials. This could be due to the lower activities injected into the radio-HPLC because of the poor RCY obtained in the majority of the experiments causing the concentration of  $^{211}\text{At}$  to be very small. Figure 3.10 shows a comparison of the RCP for Trial At-2, Trial At-7 and Trial At-9.

#### 3.3.2 NIS

There were two sets of experiments conducted with  $^{211}\text{At}$  in which the amount of excess NIS solution was varied. The first set of experiments were conducted with a stock ATE-P-1095 in chloroform that yielded 43 nmoles of ATE-P-1095 when 3  $\mu\text{l}$  of solution were used in the experiment. The second was another stock solution that yielded 54 nmoles of ATE-P-1095 for the same volume of solution. Excessive amounts of excess NIS solution were used in the first set of experiments, figure 3.11. The peak occurred at, the lowest value 86 nmoles of excess NIS solution, for

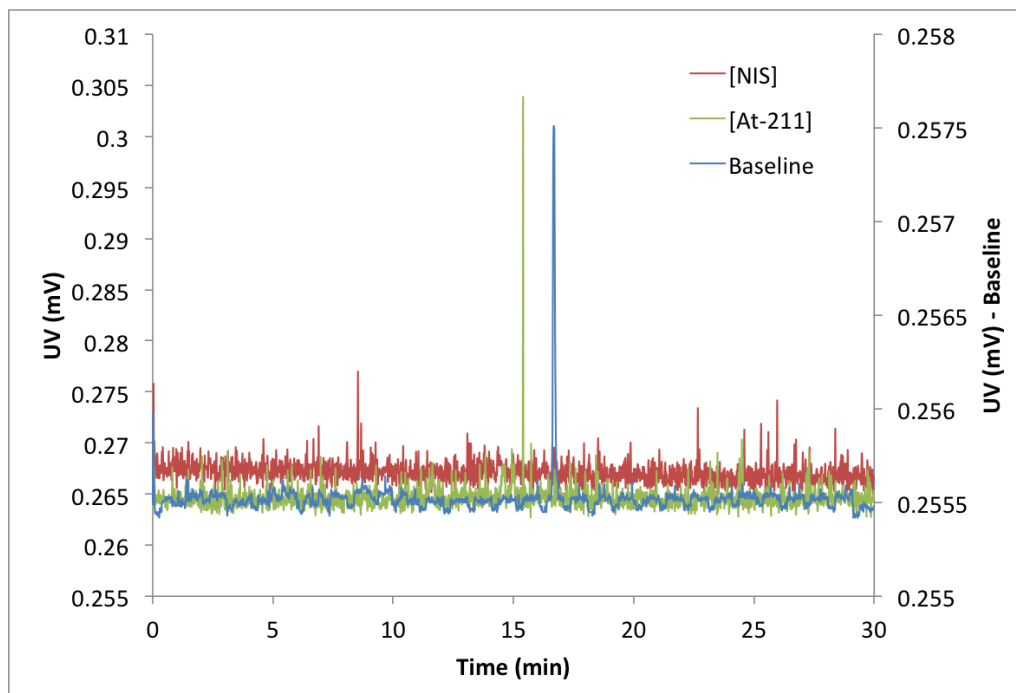


**Figure 3.10:** A radio-HPLC spectra comparing the influence of excess *NIS* solution, high radioactivity on the RCP of [ $^{211}\text{At}$ ]-MAP-1095

both specific activity and the radiochemical yield. There was an inverse relationship between the variables, as the specific activity and radiochemical yield continued decreasing as the amount of excess *NIS* increased. This is probably due to competitive binding between the iodine from the *NIS* and the  $^{211}\text{At}$ . The molar amount of *NIS* exceeded the amount of  $^{211}\text{At}$  by many orders of magnitude.

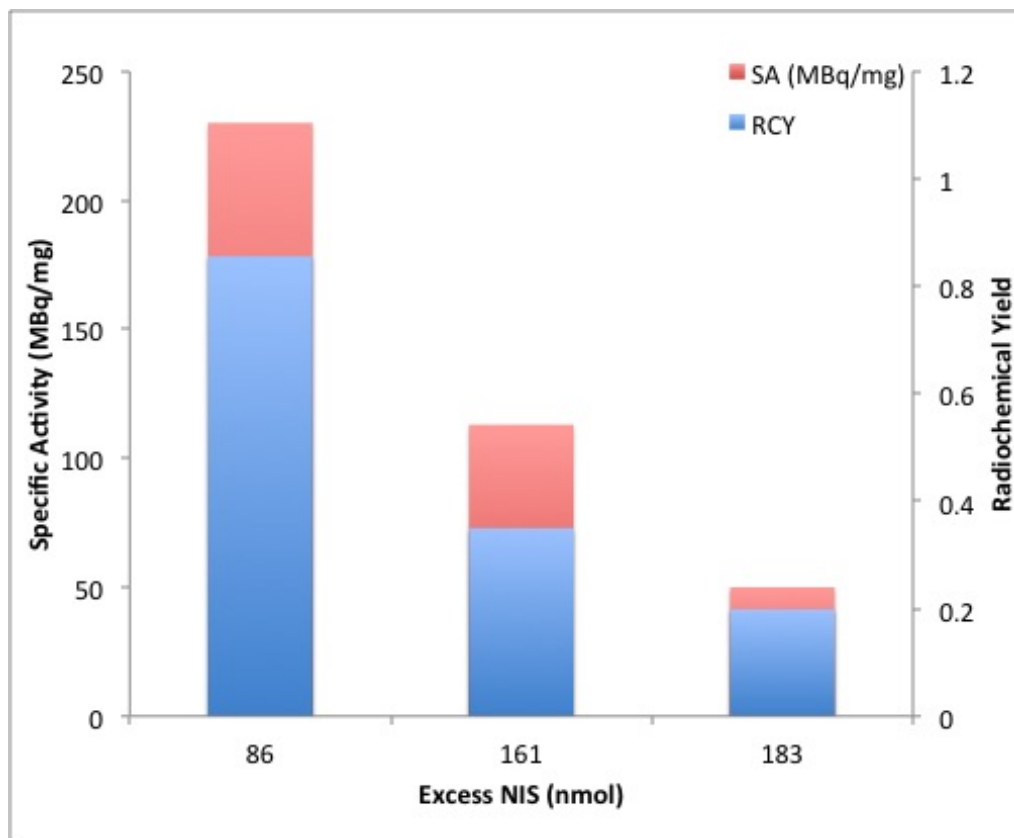


**Figure 3.11:** A comparative plot showing the influence of excess NIS on the radiochemical yield and specific activity of [ $^{211}\text{At}$ ]-MAP-1095 with a starting molar amount of 43 nmoles MAP-1095

The second set of experiments yielded a peak radiochemical yield and specific activity at 56 nmoles of excess *NIS* solution, shown in figure 3.12. The highest radiochemical yield obtained with the higher concentration, 54 nmole of ATE-P-1095, was only 50% compared to over 80% for 43 nmole of ATE-P-1095 experiments. The peak occurred at a lower molar concentration of excess *NIS* solution for the experiments with higher molar concentrations of ATE-P-1095. This is unexpected since the increased amount of ATE-P-1095 would need more iodine molecules for substitution. Increased radiochemical yields and specific activities might have been achievable at the lower molar concentration of ATE-P-1095 with molar concentrations of excess *NIS* solution closer to that of  $^{211}\text{At}$  to prevent competitive binding.

There was also large inconsistencies in the astatine labeling experiments as two experiments with the same parameters with an excess of 72 nmoles and 75 nmoles yielded a 45% difference in the radiochemical yield. The only difference was the wash volume used to activate the columns and after adding the reaction solution to the column, 2 ml versus 3 ml. The wash volume amount did not appear to influence the iodine labeling results but could have a more substantial influence on the astatine labeled molecule. More experiments would need to be run in triplicate to establish the experimental error of the system as it appears to be large.

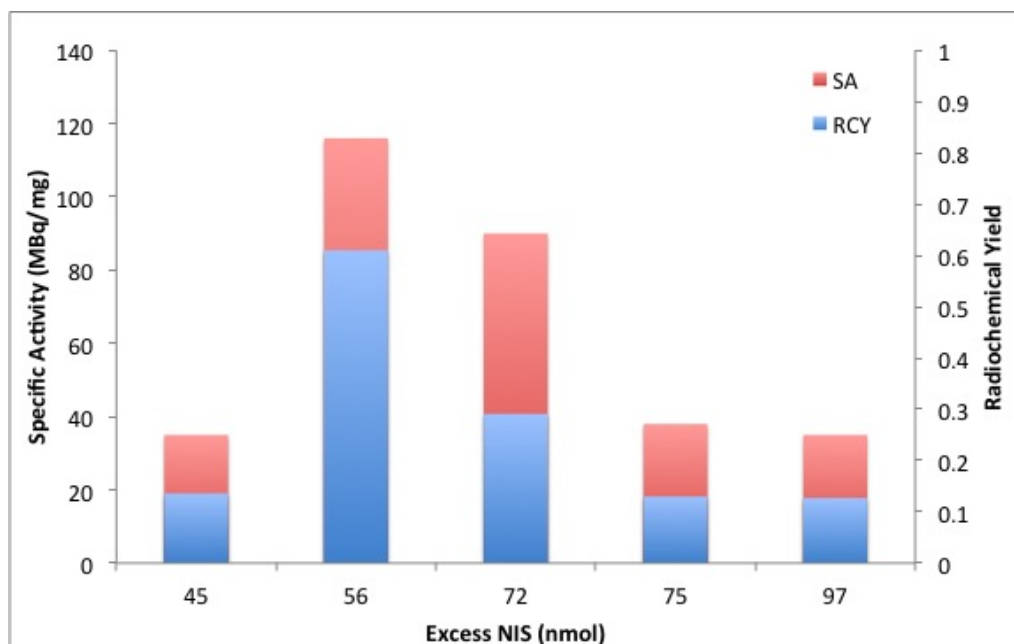


**Figure 3.12:** A comparative plot showing the influence of excess NIS on the radiochemical yield and specific activity of [ $^{211}\text{At}$ ]-MAP-1095 with a starting molar amount of 54 nmoles ATE-P-1095

### 3.3.3 Initial amount of $^{211}\text{At}$

Changing the initial amount of radioactivity increased the specific activity of the iodine labeled compound substantially and had minimal effect on the radiochemical yields of the process. The amount of  $^{211}\text{At}$  was doubled to get a starting activity of 20 MBq instead of 10 MBq. This increase in activity lead to severely decreased radiochemical yields and specific activity. Multiple elutions were done in an attempt to recover more radioactivity from the column but no significant amounts of radioactivity were recovered. Nearly 60% of the initial activity remained in the column at the end of the experiment, with about 13% coming out in the waste.

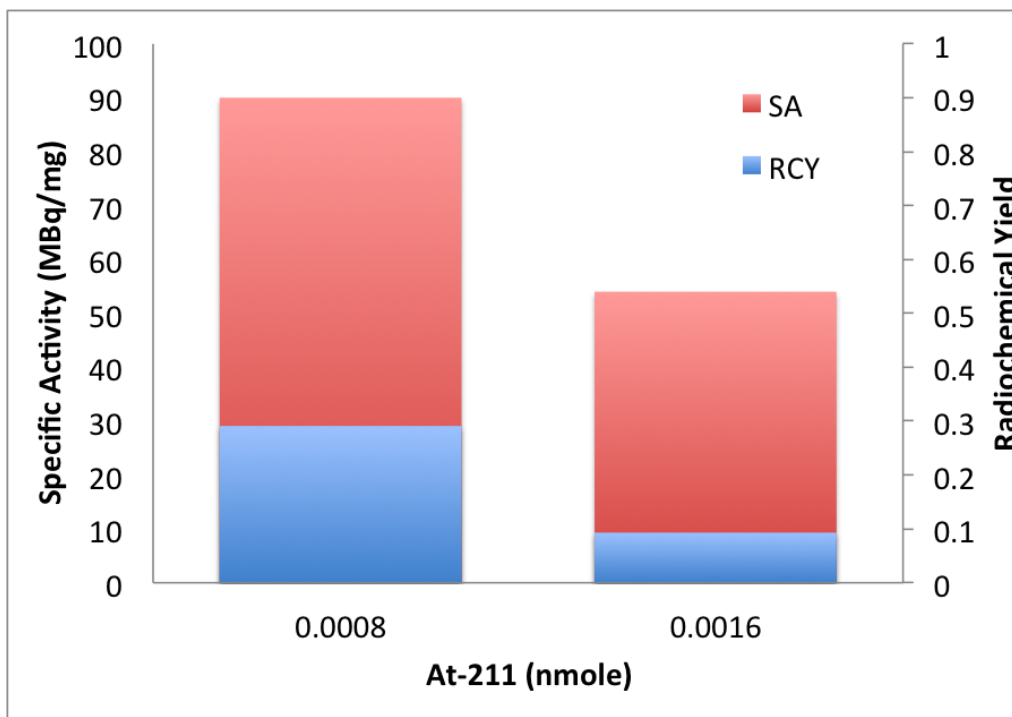


**Figure 3.13:** A comparative plot showing the influence of the molar amount of  $^{211}\text{At}$  on the radiochemical yield and specific activity of  $[\text{}^{211}\text{At}]\text{-MAP-1095}$

### 3.4 Comparison between $^{211}\text{At}$ and $^{125}\text{I}$

The chemistry of  $^{211}\text{At}$  is not as well defined as  $^{125}\text{I}$ . It was originally believed that since  $^{211}\text{At}$  is a halogen that it behaves like iodine. Since it is the heaviest of all the halogens it is expected to exhibit a more electropositive character and it is considered to have some metallic properties, like polonium. This could explain some of the differences in the results obtained from iodine and astatine. While the radio-HPLC had very similar results for both iodine and astatine there were some noticeable difference in the UV spectrum. Both compounds had single peaks at 15 minutes if there was no air in the column, but there was tailing in the majority of iodine labeled compound and more chemical impurities noticeable in the UV spectrum.

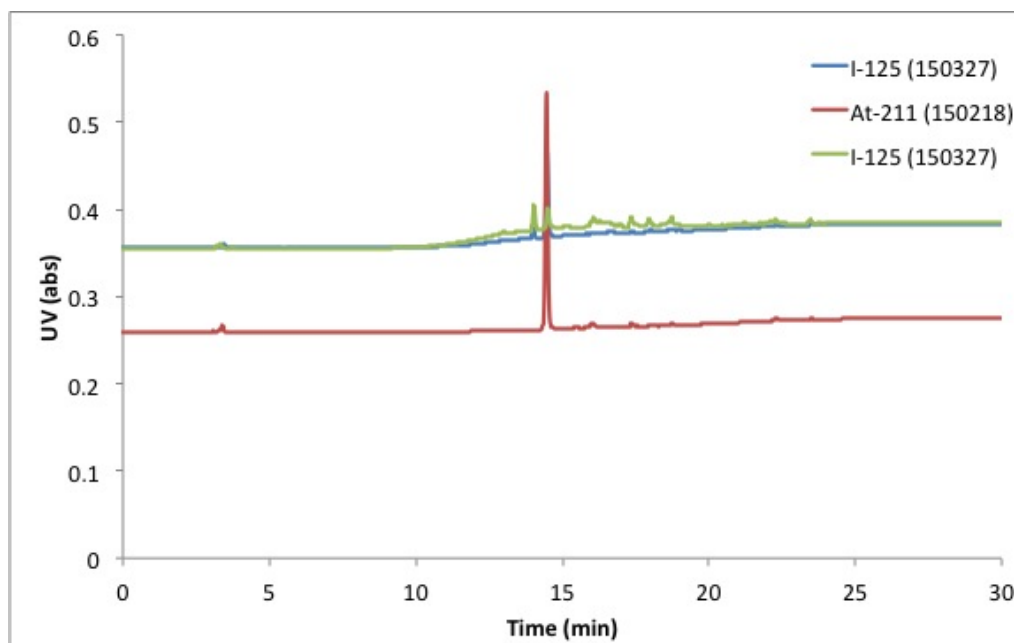


**Figure 3.14:** A comparative plot showing the differences in the HPLC spectrum between [ $^{211}\text{At}$ ]-MAP-1095 and activity of [ $^{125}\text{I}$ ]-MIP-1095

There were also minor difference in the radiation spectrum. Many of the astatine spectra had a larger amount of noise, especially at the lower activities. The low activities achieved with astatine lead to smaller overall peaks and thus more noticeable background radiation.

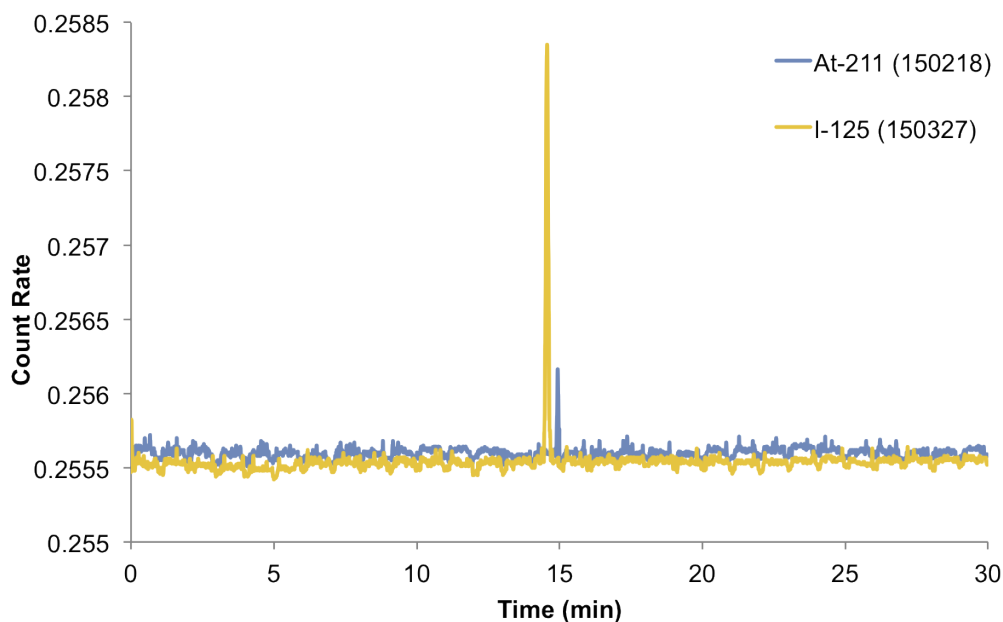


**Figure 3.15:** A comparative plot showing the differences in the radiation spectrum between  $^{211}\text{At}$ -MAP-1095 and activity of [ $^{125}\text{I}$ ]-MAP-1095

### 3.5 Cell Binding

A series of cell binding assays were conducted for both astatine and iodine. All of the experiments were done in triplicate and an average value was used to calculate the  $B/T$ . The experimental error ranged from 1%-4% for the [ $^{211}\text{At}$ ]-MAP-1095 and below 1% for the [ $^{125}\text{I}$ ]-MIP-1095. The full data set for both experiments can be found in Appendix D.

The stock solution of [ $^{211}\text{At}$ ]-MAP-1095 was diluted by a factor of 5 and 25 yielding 3 different concentrations. For [ $^{125}\text{I}$ ]-MIP-1095 one concentration was used following the same procedure used for [ $^{211}\text{At}$ ]-MAP-1095 stock solution. The solution of  $^{125}\text{I}$ -MAP-1095 in ethanol had a higher initial concentration than the [ $^{211}\text{At}$ ]-MAP-1095 due to better RCY for the experiment. This led to a higher concentration stock solution for the [ $^{125}\text{I}$ ]-MIP-1095.  $^{211}\text{At}$  has a very short half-life compared to  $^{125}\text{I}$  so to achieve the same radioactivity less  $^{211}\text{At}$  is needed when the solution is fresh. Table 3.3 is a summary of the average counts before and after binding, as well as the average  $B/T$ , for  $^{211}\text{At}$  and  $^{125}\text{I}$  at room temperature.

**Table 3.3:** Summary of cell binding labeling experiments for  $^{211}\text{At}$  and  $^{125}\text{I}$  at room temperature

	Amount (pmol)	Before		After		Average B/T
		Average Counts	Average CPM	Average Counts	Average CPM	
At	0.0360	47811	96657	2942	5864	0.0615
	0.0069	9248	18512	1977	3932	0.2137
	0.0014	1844	3665	594	1165	0.3224
I	30.00	129679	406469	33208	100693	0.2561

The highest  $B/T$  for [ $^{211}\text{At}$ ]-MAP-1095 was seen at the lowest concentration and decreased as the molar amount of [ $^{211}\text{At}$ ]-MAP-1095 in the solution increased, shown in figure 3.16. This is conducive with what was expected as there are more available binding spots for the [ $^{211}\text{At}$ ]-MAP-1095 at lower activities. The amount of radioactivity sticking to the test tubes was found to be around 0.5% for the highest concentration of [ $^{211}\text{At}$ ]-MAP-1095 and was not considered to be a significant contributing factor to the bound activity.

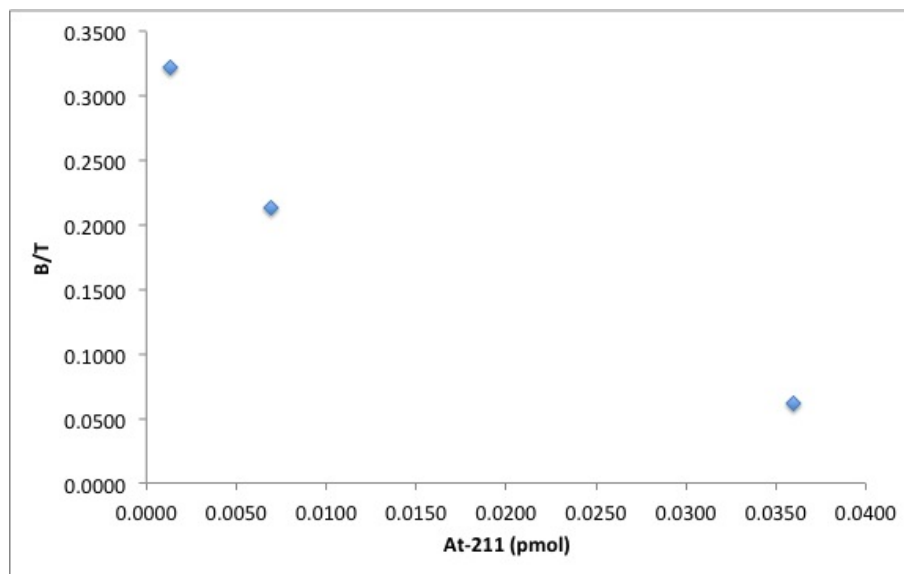


**Figure 3.16:** A comparative plot showing the influence of the amount of  $^{211}\text{At}$  on the  $B/T$  of [ $^{211}\text{At}$ ]-MAP-1095 to LNCaP cells.

The [ $^{125}\text{I}$ ]-MIP-1095 yielded a fairly high  $B/T$  in comparison to [ $^{211}\text{At}$ ]-MAP-1095, 25.6%, even though the amount of [ $^{125}\text{I}$ ]-MIP-1095 was 3-5 orders of magnitude higher. Another set of experiments were conducted with [ $^{125}\text{I}$ ]-MIP-1095 to see the influence of concentration and temperature on the cell binding. Some cells internalize certain molecules and then excrete them. This can lead to lower overall  $B/T$  if the time frame in which this occurs is less than that of the incubation time. Internalization can be minimized or slowed if the cells are put in an ice bath during the incubation. Table 3.4 is a summary of the average counts before and after binding, as well as the average  $B/T$ , for  $^{125}\text{I}$  at room temperature and in an ice bath.

**Table 3.4:** Summary of cell binding labeling experiments for  $^{125}\text{I}$  at room temperature and in an ice bath

	Amount (pmol)	Before		After		Average B/T
		Average Counts	Average CPM	Average Counts	Average CPM	
On Ice	69.5	863142	948137	59923	59923	0.0694
	13.7	182723	186422	31789	31878	0.1740
Room Temp.	70.7	869047	964478	71900	59211	0.0827
	13.9	185298	189114	59211	59776	0.3195

There was a 16% difference in the  $B/T$  at the high concentration between the room temperature and the ice bath. The difference grew to 45% for the lower concentration in favor of the room temperature binding. Figure 3.17 shows a comparison at the two concentrations for the two temperatures. The small difference at 70 pmole of [ $^{125}\text{I}$ ]-MIP-1095 is likely due to there being a limited number of binding spots per individual [ $^{125}\text{I}$ ]-MIP-1095 molecule. There was likely minimal internalization and excretion of the  $^{125}\text{I}$ , but the same conclusion cannot be drawn for  $^{211}\text{At}$  due

### 3. Results

---

to the differences in the way the radionuclides interact with the body.

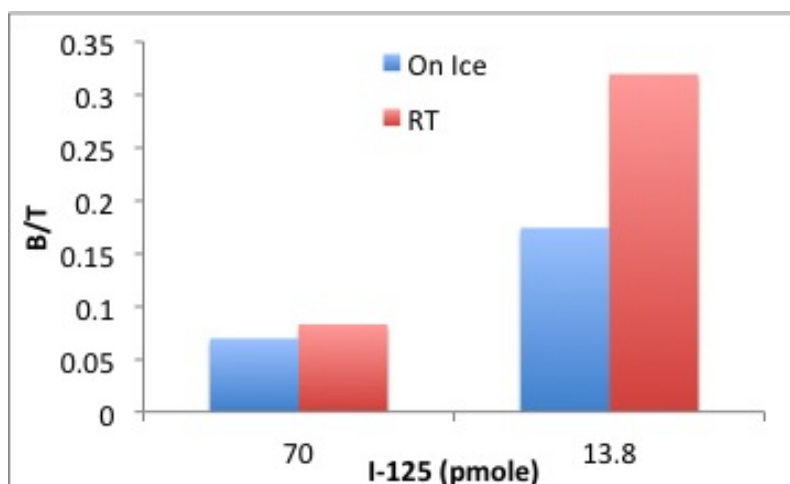


**Figure 3.17:** A comparative plot showing the influence of the temperature on the  $B/T$  of  $^{125}\text{I}$ -MAP-1095 to LNCaP cells.

The concentrations for each of the [ $^{125}\text{I}$ ]-MIP-1095 cell binding experiments conducted at room temperature were compared in Figure 3.18. The [ $^{125}\text{I}$ ]-MIP-1095 cell binding experiments exhibited results similar to the [ $^{211}\text{At}$ ]-MAP-1095 cell binding experiments in regard to the influence of concentration on the  $B/T$ . There appears to be a linear fit to the [ $^{125}\text{I}$ ]-MIP-1095 cell binding curve, whereas the [ $^{211}\text{At}$ ]-MAP-1095 cell binding curve appears to follow an exponential trend. A direct comparison cannot be made since the order of magnitude of the concentrations differs so greatly. A series of  $^{125}\text{I}$ -MIP-1095 cell binding studies at lower concentrations could provide a more complete picture.

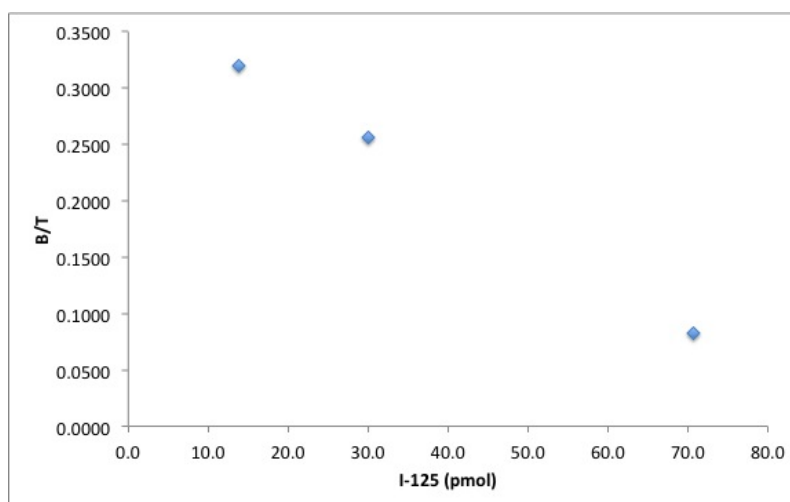


**Figure 3.18:** A comparative plot showing the influence of the amount of  $^{125}\text{I}$  on the  $B/T$  of [ $^{125}\text{I}$ ]-MIP-1095 to LNCaP cells.

The relatively low binding yield for each of the experiments, and the increased binding for lower concentration solutions is explained by the ratio of the number of [ $^{125}\text{I}$ ]-MIP-1095 and [ $^{211}\text{At}$ ]-MAP-1095 molecules to the number of LNCaP cells, shown in Table 3.5. The first set of experiments were done with an initial cell concentration of  $6.67 \times 10^6$  to  $1.33 \times 10^7 \text{ cells/ml}$  which was further diluted to  $3.33 \times 10^6$  to  $6.67 \times 10^6 \text{ cells/ml}$ . This led to a very low cell count per test tube, each tube only had  $200 \mu\text{l}$  of cell solution, in comparison to the number of [ $^{125}\text{I}$ ]-MIP-1095 and [ $^{211}\text{At}$ ]-MAP-1095 molecules. As the ratio decreases the  $B/T$  values increase. An ideal binding experiment would be one in which the cells were in excess.

**Table 3.5:** Summary of calculations for the ratio of the number of  $^{125}\text{I}$ -MIP-1095 and  $^{211}\text{At}$ -MAP-1095 molecules to the number of LNCaP cells.

	# of bindable molecules	# of LNCaP Cells		Ratio	
		Low	High	Low	High
At	2.17E+11	6.67E+05	1.33E+06	3.25E+05	1.63E+05
	4.15E+10	6.67E+05	1.33E+06	6.23E+04	3.12E+04
	8.22E+09	6.67E+05	1.33E+06	1.23E+04	6.17E+03
I	1.80573E+14	6.67E+05	1.33E+06	2.71E+08	1.35E+08

The same trend can be seen in the second set of experiments testing the internalization of the [ $^{125}\text{I}$ ]-MIP-1095 and [ $^{211}\text{At}$ ]-MAP-1095 molecules in the LNCaP cells, shown in Figure 3.6. The initial LNCaP cell concentration was higher ( $1 \times 10^7 \text{ cells/ml}$ ) and a volume of  $300 \mu\text{l}$  was added to each of the vials. This resulted in a number of cells per experiment that was 2-4x the previous experiments. However, this did not appear to have a huge influence on the results since the concentration of the [ $^{125}\text{I}$ ]-MIP-1095 was more than 2x higher than the previous experiments. There was a slight improvement in the  $B/T$  for the x5 dilution which yielded a lower ratio of bindable molecules to LNCaP cells.

**Table 3.6:** Summary of calculations for the ratio of the number of  $^{125}\text{I}$ -MIP-1095 molecules to the number of LNCaP cells.

	# of bindable molecules	# of LNCaP Cells	Ratio
On Ice	4.18E+14	3.00E+06	1.39E+08
	8.23E+13	3.00E+06	2.74E+07
Room Temp.	4.26E+14	3.00E+06	1.42E+08
	8.34E+13	3.00E+06	2.78E+07

### 3.6 Comparison with K. Maresca

A comparison was done with the results obtained from K. Maresca [17]. Briefly, ATE-P-1095 was radiolabeled with  $^{123}\text{I}$  and  $^{131}\text{I}$  via  $\text{Na}^{123}\text{I}$  and  $\text{Na}^{131}\text{I}$ . Iodogen was used as the oxidant and the boc-protecting groups were removed using TFA. The lead compounds were radioiodinated in  $\geq 60\%$  radiochemical yield with  $>95\%$

### 3. Results

---

radiochemical purity following purification by reverse phase high pressure liquid chromatography with a specific activity of  $> 4000 \text{ mCi}/\mu\text{mol}$ [17]. In comparison with the results obtained in these experiments of radiochemical yields  $\geq 95\%$  with radiochemical purities  $\geq 99\%$  and a maximum specific activity of  $694 \text{ mCi}/\mu\text{mol}$ . The large difference in specific activity is likely due to the differences in half-lives between the iodine species and the amount of initial radioactive  $\text{NaI}$ . The half-life of both  $^{123}\text{I}$  and  $^{131}\text{I}$  are 13.22 hours and 8.02 days in comparison to 60 days for  $^{125}\text{I}$  making them substantially more radioactive for smaller masses.

# 4

## Conclusion

High radiochemical purities are achievable for both [ $^{125}\text{I}$ ]-MIP-1095 and [ $^{211}\text{At}$ ]-MAP-1095. RCP greater than 99% were observed for all [ $^{125}\text{I}$ ]-MIP-1095 experiments and equally high RCP values were observed in the majority of [ $^{211}\text{At}$ ]-MAP-1095 experiments, though there was a lot of noise in observed in the baseline making absolute quantification of the RCP for [ $^{211}\text{At}$ ]-MAP-1095 difficult in some experiments. The RCP is a very important aspect of quality control for a radiopharmaceutical, impurities can have unwanted side effects and may result in increased radiation dose to healthy tissue.

The radiochemical yield for the [ $^{125}\text{I}$ ]-MIP-1095 experiments did not appear to be influenced heavily by the amount of excess NIS solution, the oxidizing agent concentration or the amount of Na[ $^{125}\text{I}$ ] added to the system. It did exhibit signs of dependence on the flow rate of the solution and eluent through the Bond Elute Plexa column. For the [ $^{125}\text{I}$ ]-MIP-1095 synthesis RCY near 100% were obtained for nearly all experiments. The synthesis of [ $^{211}\text{At}$ ]-MAP-1095 did not yield the same consistent results in regards to RCY as its [ $^{125}\text{I}$ ]-MIP-1095 counterpart. A RCY of 85.6% was obtained showing that it is possible to get good yields from the synthesis, but reproducibility of this was low and most of the values for RCY were around 30%. The RCY for [ $^{211}\text{At}$ ]-MAP-1095 can likely be increased by substantially reducing the amount of excess NIS used. This will minimize the competitive binding between iodine and  $^{211}\text{At}$ .

The maximization of the specific activity for [ $^{125}\text{I}$ ]-MIP-1095 was obtained through varying the amount of excess NIS solution, the oxidizing agent concentration or the amount of Na[ $^{125}\text{I}$ ] added to the system. Unlike the RCY yield, the specific activity showed sensitivity to the amount of excess NIS and the concentration of chloramine-T, favoring a moderate amount of each. The SA had the highest sensitivity to the amount of Na[ $^{125}\text{I}$ ] added. The increase of Na[ $^{125}\text{I}$ ] to 3x the value added to all prior experiments, increasing the activity from an average of 10 MBq to 30 MBq, resulted in a 3x increase in SA. This indicates that the specific activity could be increased further as the amount of Na[ $^{125}\text{I}$ ] is the limiting factor.

Large specific activities were also something that was not readily obtainable with the [ $^{211}\text{At}$ ]-MAP-1095 experiments. This is likely due to the poor RCY of the majority of the experiments. Most of the radioactivity remained bound to the column or, at times, was lost in the waste stream. The influence of the amount of excess NIS solution on the RCY and SA indicated that the ideal values were when the molar

#### 4. Conclusion

---

amount of excess NIS was almost equal to the molar amount of added ATE-P-1095 but no definite conclusions can be made. The increase of the amount of  $^{211}\text{At}$  exhibited the opposite behavior of the  $[^{125}\text{I}]$ -MIP-1095 synthesis. The increase of  $^{211}\text{At}$  by 2x reduced both the RCY and the SA by 3x. This indicated that the limiting factor was not the  $^{211}\text{At}$ .

The cell binding experiments showed  $B/T$  values between 6% -33% for both  $[^{125}\text{I}]$ -MIP-1095 and  $[^{211}\text{At}]$ -MAP-1095. For both molecules the  $B/T$  went up as the concentration decreased. This was expected as the ratio of  $[^{125}\text{I}]$ -MIP-1095 and  $[^{211}\text{At}]$ -MAP-1095 molecules to the LNCaP cells was a 3-8 orders order of magnitude difference. There was an insufficient number of binding spots for each of the  $[^{125}\text{I}]$ -MIP-1095 and  $[^{211}\text{At}]$ -MAP-1095 molecules. The internalization of the  $[^{125}\text{I}]$ -MIP-1095 was also examined. Two identical binding experiments were conducted, one at room temperature and one in an ice bath. Putting the cells on ice can slow or stop the internalization and excretion of the  $[^{125}\text{I}]$ -MIP-1095 from the LNCaP cell. The  $B/T$  values for the room temperature experiments at the diluted concentration were double the  $B/T$  values for the diluted concentration experiments kept on ice during the incubation period, indicating that the  $[^{125}\text{I}]$ -MIP-1095 was not being excreted from the cell. This might not be the case for  $[^{211}\text{At}]$ -MAP-1095 as the two molecules could have different physiological behaviors in the body.

Overall high specific activities, radiochemical yield and a high radiochemical purity was achievable for  $[^{125}\text{I}]$ -MIP-1095. This is promising for use in treating micrometastases in prostate cancer due to the Auger electrons emitted during decay and that it is more readily available than  $^{211}\text{At}$  because of its long half-life. The  $[^{125}\text{I}]$ -MIP-1095 proved to be stable with no degradation for weeks at a time so it can be made in larger quantities and stored until needed. Experimentation showed that a high radiochemical purity can be achieved for  $[^{211}\text{At}]$ -MAP-1095, and relatively high radiochemical yields and specific activities were shown to be possible. With further experimentation yielding a deeper understanding of the mechanisms and synthesis of  $[^{211}\text{At}]$ -MAP-1095 better yield and higher specific activities can be obtained.

Future recommendations would be to substantially decrease the amount of NIS in the 1% acetic acid in methanol added in the second step of the astatination protocol. This should decrease the competitive binding between the iodine from the NIS and the  $^{211}\text{At}$ . All of the radiohalogenation experiments should be done in triplicate to establish the amount of experimental error as it appears to be rather large for the  $^{211}\text{At}$  labelings. More cell binding studies should be done with either increased numbers of cells or reduced concentration of the  $[^{125}\text{I}]$ -MIP-1095 and  $[^{211}\text{At}]$ -MAP-1095. This will ensure there is enough binding spots available for the  $[^{125}\text{I}]$ -MIP-1095 and  $[^{211}\text{At}]$ -MAP-1095.

# Bibliography

- [1] American Cancer Society, Inc., Surveillance Research; Cancer Facts & Figures, 2015.
- [2] Held, K. (2006). Radiobiology for the Radiologist, 6th ed., by Eric J. Hall and Amato J. Giaccia. Radiation Research, 166(5), pp.816-817.
- [3] Suit, H., Goldberg, S., Niemierko, A., Ancukiewicz, M., Hall, E., Goitein, M., Wong, W. and Paganetti, H. (2007). Secondary Carcinogenesis in Patients Treated with Radiation: A Review of Data on Radiation-Induced Cancers in Human, Non-human Primate, Canine and Rodent Subjects. Radiation Research, 167(1), pp.12-42.
- [4] Schneider, U. (2011). Modeling the Risk of Secondary Malignancies after Radiotherapy. Genes, 2(4), pp.1033-1049.
- [5] Bushberg, et al. The Essential Physics of Medical Imaging, 2nd ed., pp. 817.
- [6] Akhtar, N., Pail, O., Saran, A., Tyrell, L. and Tagawa, S. (2012). Prostate-Specific Membrane Antigen-Based Therapeutics. Advances in Urology, 2012, pp.1-9.
- [7] OSEH: Radionuclide Safety Data Sheets - I-125. [online] Available at: <http://www.oseh.umich.edu/radiation/I125.shtml> [Accessed 10 May 2015].
- [8] Chang, J.: Table of Nuclides, KAERI(Korea Atomic Energy Research Institute). Available at: <http://atom.kaeri.re.kr/ton/>. Retrieved 2015.
- [9] Wilicka M.A, Adelstein S.J., Kassis A.I. (1998). Indirect mechanisms contribute to biological effects produced by decay of DNA-incorporated iodine-125 in mammalian cell in *vitro*: double-strand breaks. *Radiat. Res.* 118, pp.1040-1046.
- [10] Rössler K. (1985). Irradiation and self-irradiation of astatine compounds. *Gmelin Handbook of inorganic chemistry-astatine* 8th ed., pp. 3500-3503.
- [11] European Community, Official Journal. (1996). 159, pp.1-114.
- [12] Alberts, B. (2002). Molecular biology of the cell. New York: Garland Science.
- [13] O'Keefe, D., Su, S., Bacich, D., Horiguchi, Y., Luo, Y., Powell, C., Zandvliet, D., Russell, P., Molloy, P., Nowak, N., Shows, T., Mullins, C., Vonder Haar, R., Fair, W. and Heston, W. (1998). Mapping, genomic organization and promoter

- analysis of the human prostate-specific membrane antigen gene. *Biochimica et Biophysica Acta (BBA) - Gene Structure and Expression*, 1443(1-2), pp.113-127.
- [14] Perner, S., Hofer, M., Kim, R., Shah, R., Li, H., Möller, P., Hautmann, R., Gschwend, J., Kuefer, R. and Rubin, M. (2007). Prostate-specific membrane antigen expression as a predictor of prostate cancer progression. *Human Pathology*, 38(5), pp.696-701.
- [15] Vallabhajosula, S. (2005). Radioimmunotherapy of Prostate Cancer Using 90Y- and 177Lu-Labeled J591 Monoclonal Antibodies: Effect of Multiple Treatments on Myelotoxicity. *Clinical Cancer Research*, 11(19), pp.7195s-7200s.
- [16] Zechmann, C., Afshar-Oromieh, A., Armor, T., Stubbs, J., Mier, W., Hadaschik, B., Joyal, J., Kopka, K., Debus, J., Babich, J. and Haberkorn, U. (2014). Radiation dosimetry and first therapy results with a 124I/131I-labeled small molecule (MIP-1095) targeting PSMA for prostate cancer therapy. *European Journal of Nuclear Medicine and Molecular Imaging*, 41(7), pp.1280-1292.
- [17] Maresca, K., Hillier, S., Femia, F., Keith, D., Barone, C., Joyal, J., Zimmerman, C., Kozikowski, A., Barrett, J., Eckelman, W. and Babich, J. (2009). A Series of Halogenated Heterodimeric Inhibitors of Prostate Specific Membrane Antigen (PSMA) as Radiolabeled Probes for Targeting Prostate Cancer. *Journal of Medicinal Chemistry*, 52(2), pp.347-357.
- [18] Lindegren, S., Jensen, H. and Jacobsson, L. (2014). A radio-high-performance liquid chromatography dual-flow cell gamma-detection system for on-line radiochemical purity and labeling efficiency determination. *Journal of Chromatography A*, 1337, pp.128-132.
- [19] Emma Aneheim, Holger Jensen, Per Albertsson, Sture Lindegren (2014) Astatine-211 labeling: a study towards automatic production of astatinated antibodies, *J Radial Nucl Chem* 303:979-983
- [20] Lindegren S., Bäck T. and Jensen H. J. (2001) Dry-distillation of Astatine-211 from Irradiated Bismuth Targets: A Time-saving procedure with High Recovery Yields. *Appl. Radiat. Isot.* 55, 157-160.
- [21] Horoszewicz JS, Leong SS, Kawinski E, Karr JP, Rosenthal H, Chu TM, Mirand EA, Murphy GP (April 1983). "LNCaP model of human prostatic carcinoma". *Cancer Res* 43 (4): 1809–18. PMID 6831420.
- [22] Choppin, G., Liljenzin, J. and Rydberg, J. (2002). *Radiochemistry and nuclear chemistry*. Woburn, MA: Butterworth-Heinemann.
- [23] *Pure and Applied Chemistry*. Volume 66, Issue 12, Pages 2513–2526, ISSN (Online) 1365-3075, ISSN (Print) 0033-4545, DOI: 10.1351/pac199466122513, January 2009

# A

## Iodination Protocol

### Reagents:

ATE-P-1095

Methanol

Chloramine-T

Ethanol

N-iodosuccinimid (NIS)

Acetic Acid (HAc)

$Na^{125}I$

MilliQ Water

Trifluoric Acid (TFA)

Citrate Buffer pH 5.5

### Equipment:

Eppendorf tubes (0.5 mL and 1.7 mL)

Borosilicate reaction vials (1.1 mL)

Bond Elut columns

Plastic syringe

Syringe - Column adapters

Pipettes and tips (0-200 microliters)

### Preparatory Work:

*In advance*

- 1% HAc in Methanol ( 25 mL)
- 0.1% HAc in MilliQ water ( 50 mL)
- 0.1 M Citrate pH 5.5 ( 500 mL)
- 20% Ethanol in MilliQ water
- If necessary make a stock solution of ATE-P in chloroform (1 mg/mL)

*Right before*

- 10 mg/mL Chloramine-T in MilliQ water ( 1 mL)
- 5-10 mM ( 1 mg/mL) in NIS 1% HAc in Methanol ( 1 mL)

## A. Iodination Protocol

---

- Wash Bond Elute column with 20% Eth/Water mixture (2-3 pre-dilution solution volumes = 2mL)

### Instructions:

1. Add ATE-P-1095 in chloroform to a glass reaction vial and evaporate to dryness under a stream of nitrogen
2. Dissolve residue in 12  $\mu$ l 1% HAc/Methanol
3. Add 1  $\mu$ l Chloramine-T solution
4. Add  $Na^{125}I$
5. Add 3  $\mu$ l excess of NIS over ATE-P-1095 to substitute remaining tin groups
6. Incubate at gentle agitation for 1 minute at room temperature
7. Resolve in 0.5 mL neat TFA to remove the tert-butyloxy carbonyl protecting groups
8. Incubate at gentle agitation for 15 minutes at room temperature
9. Dilute with 5 mL MilliQ water
10. Optional to take a midpoint sample for the HPLC
11. Add the reaction mixture to the Bond Elute column
12. Wash the column with 20% ethanol/water mixture - (2-4 pre-dilution solution volumes = 2 mL)
13. Dry the column with air in the syringe
14. Elute product with 500  $\mu$ l of 95% ethanol
15. Evaporate with nitrogen stream and resolve in 0.1 M Citrate buffer pH 5.5 (*For Injection*)

# B

## Astatination Protocol

### Reagents:

ATE-P-1095

Methanol

Ethanol

N-iodosuccinimid (NIS)

Acetic Acid (HAc)

$^{211}\text{At}$ /chloroform

MilliQ Water

Trifluoric Acid (TFA)

Citrate Buffer pH 5.5

### Equipment:

Eppendorf tubes (0.5 mL and 1.7 mL)

Borosilicate reaction vials (1.1 mL)

Bond Elut columns

Plastic syringe

Syringe - Column adapters

Pipettes and tips (0-200 microliters)

### Preparatory Work:

*In advance*

- 1% HAc in Methanol ( 25 mL)
- 0.1% HAc in MilliQ water ( 50 mL)
- 0.1 M Citrate pH 5.5 ( 500 mL)
- 20% Ethanol in MilliQ water
- If necessary make a stock solution of ATE-P in chloroform (1 mg/mL)

*Right before*

- 10 mg/mL Chloramine-T in MilliQ water ( 1 mL)
- 5-10 mM ( 1 mg/mL) in NIS 1% HAc in Methanol ( 1 mL)

## B. Astatination Protocol

---

- Wash Bond Elute column with 20% Eth/Water mixture (2-3 pre-dilution solution volumes = 2mL)

### **Instructions:**

1. Add ATE-P-1095 in chloroform to a glass reaction vial and evaporate to dryness under a stream of nitrogen
2. Dissolve residue in 12  $\mu\text{l}$  NIS (1 mg/ml) in 1% HAc/Methanol
3. Add  $^{211}\text{At}$  in chloroform to a clean vial and evaporate to dryness under a stream of nitrogen
4. Incubate at gentle agitation for 1 minute at room temperature
5. Add 3  $\mu\text{l}$  excess of NIS over ATE-P-1095 to substitute remaining tin groups
6. Incubate at gentle agitation for 1 minute at room temperature
7. Resolve in 0.5 mL neat TFA to remove the tert-butyloxy carbonyl protecting groups
8. Incubate at gentle agitation for 15 minutes at room temperature
9. Dilute with 5 mL MilliQ water
10. Optional to take a midpoint sample for the HPLC
11. Add the reaction mixture to the Bond Elute column
12. Wash the column with 20% ethanol/water mixture - (2-4 pre-dilution solution volumes = 2 mL)
13. Dry the column with air in the syringe
14. Elute product with 500  $\mu\text{l}$  of 95% ethanol
15. Evaporate with nitrogen stream and resolve in 0.1 M Citrate buffer pH 5.5 (*For Injection*)

# C

## Radio-HPLC Spectra

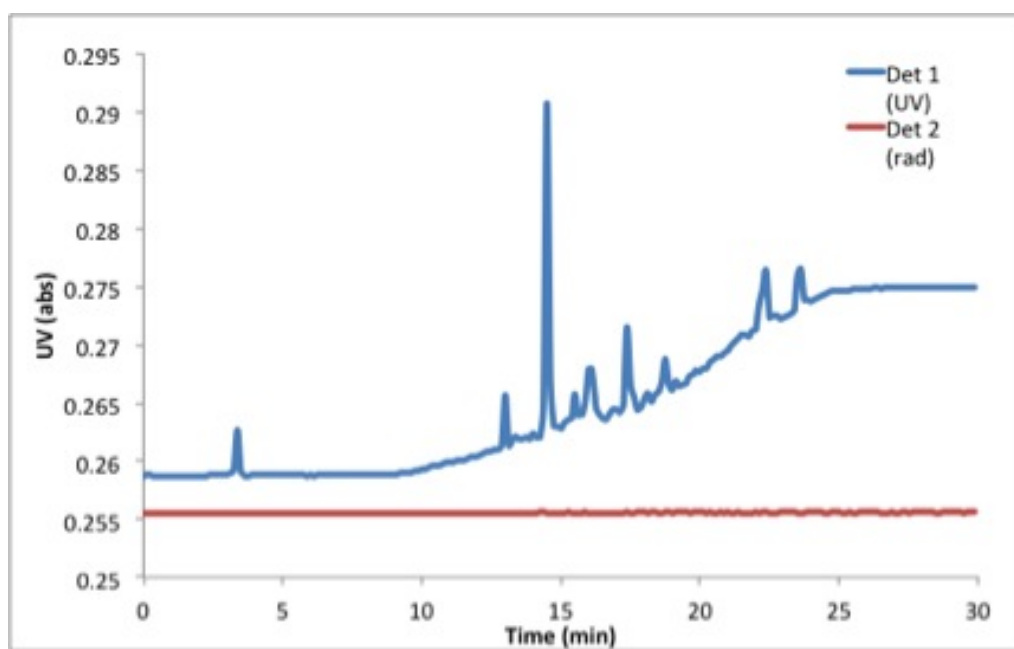


**Figure C.1:** HPLC spectrum for product A, conducted on 2015/02/02, [ $^{125}I$ ]-MIP-1095

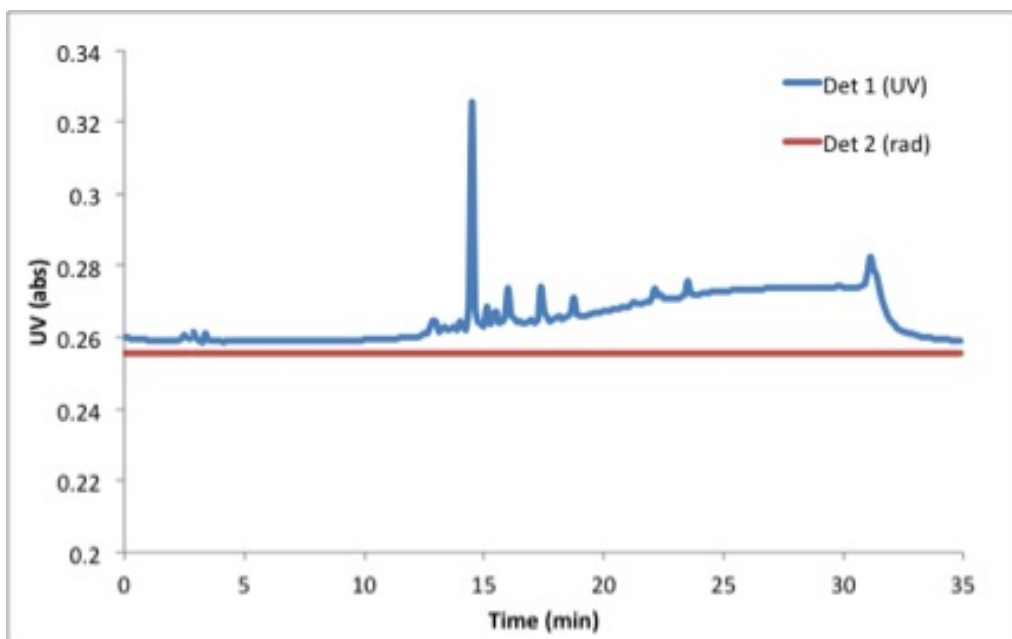


**Figure C.2:** HPLC spectrum for product B, conducted on 2015/02/02, [ $^{125}\text{I}$ ]-MIP-1095

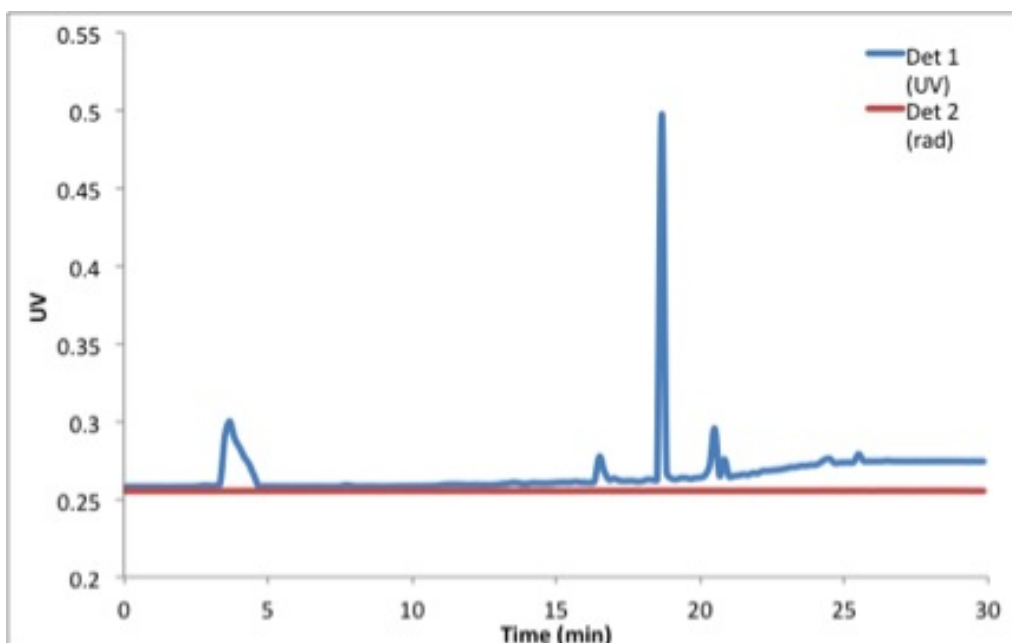


**Figure C.3:** HPLC spectrum for sample A, conducted on 2015/02/02, [ $^{125}\text{I}$ ]-MIP-1095

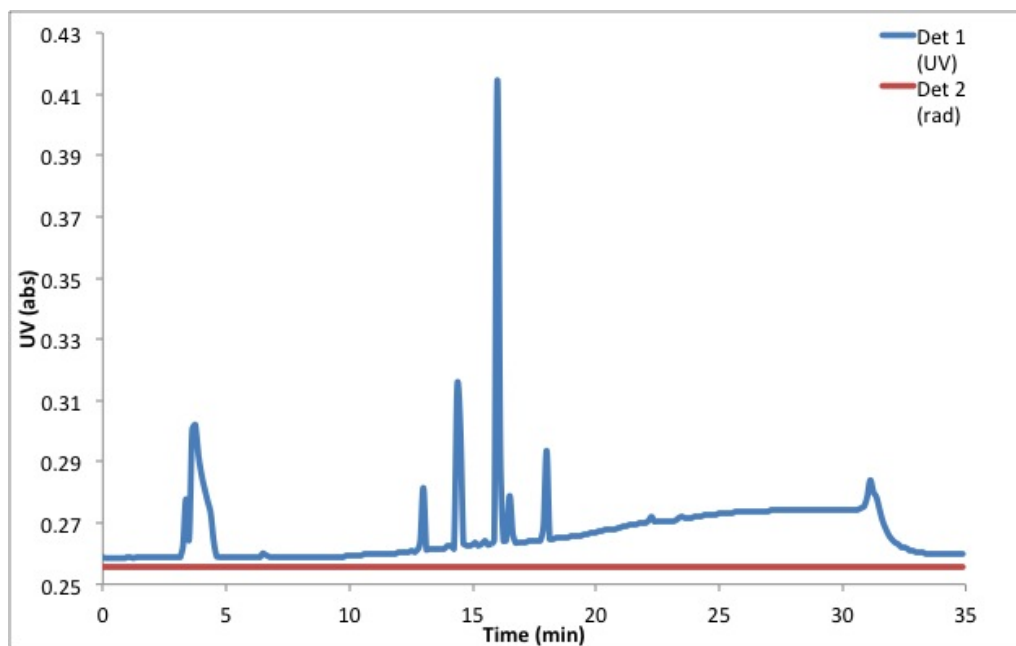


**Figure C.4:** HPLC spectrum for sample B, conducted on 2015/02/02, [ $^{125}\text{I}$ ]-MIP-1095

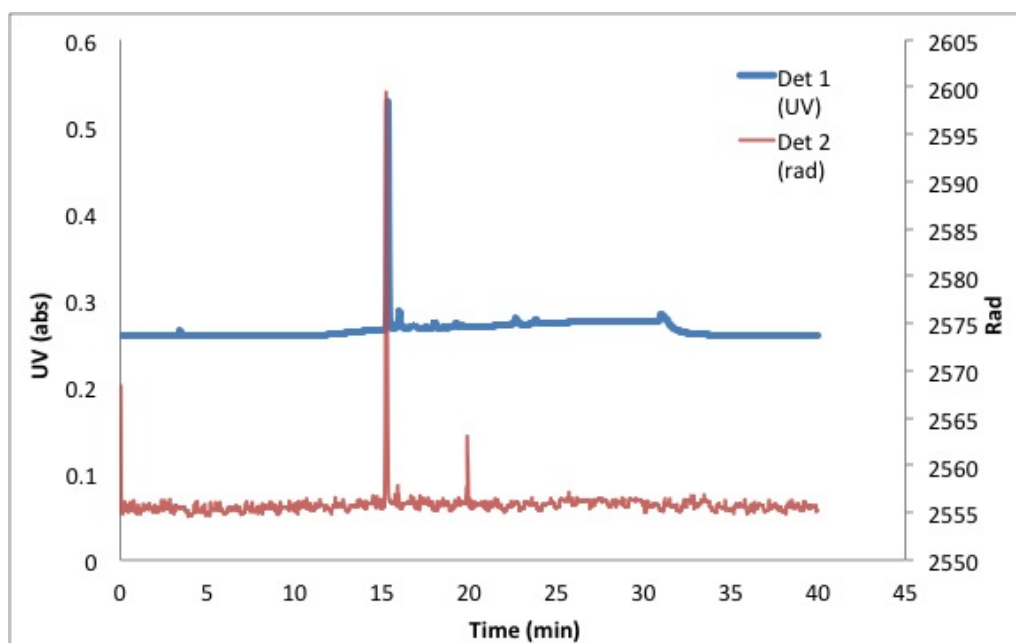


**Figure C.5:** Radio-HPLC spectrum for the product, conducted on 2015/02/11, [ $^{211}\text{At}$ ]-MAP-1095

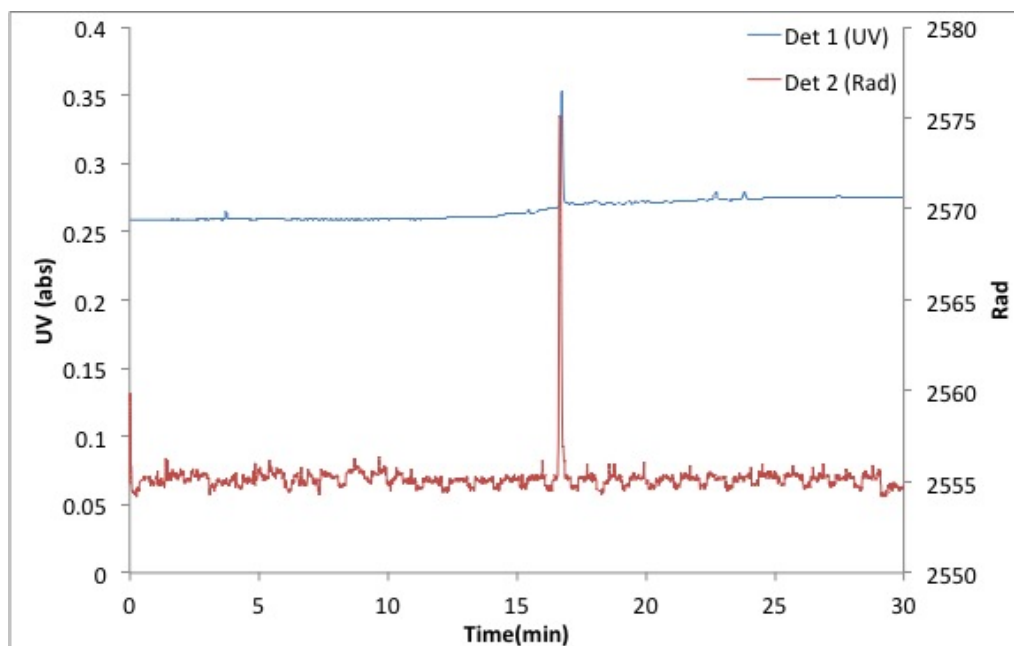


**Figure C.6:** Radio-HPLC spectrum for the product 1 immediately after synthesis, conducted on 2015/02/18, [  $^{211}\text{At}$ ]-MAP-1095

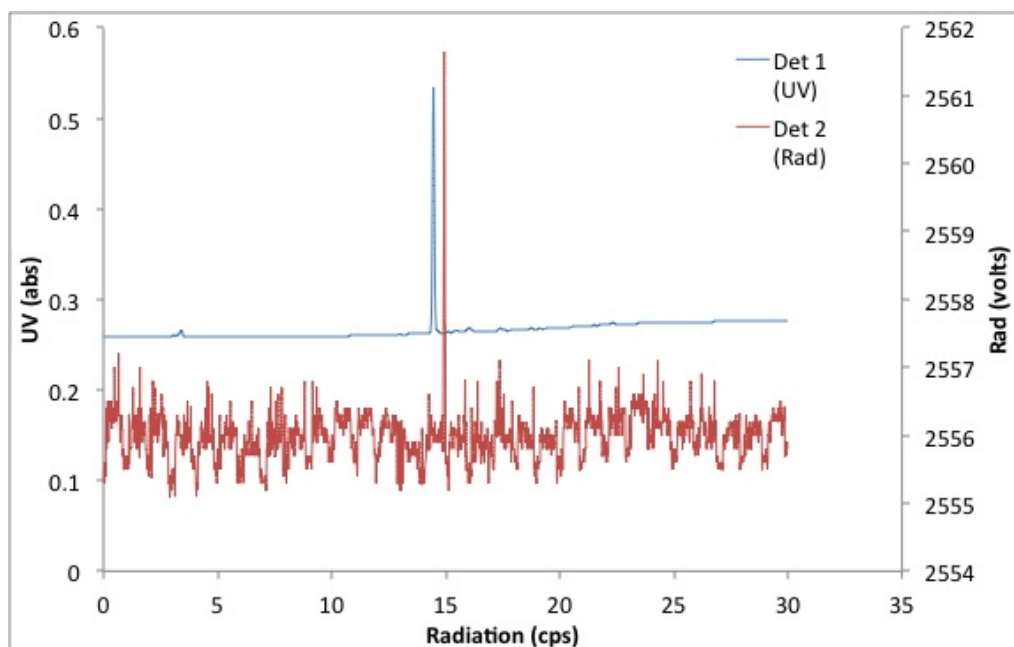


**Figure C.7:** Radio-HPLC spectrum for the product 2 immediately after synthesis, conducted on 2015/02/18, [  $^{211}\text{At}$ ]-MAP-1095

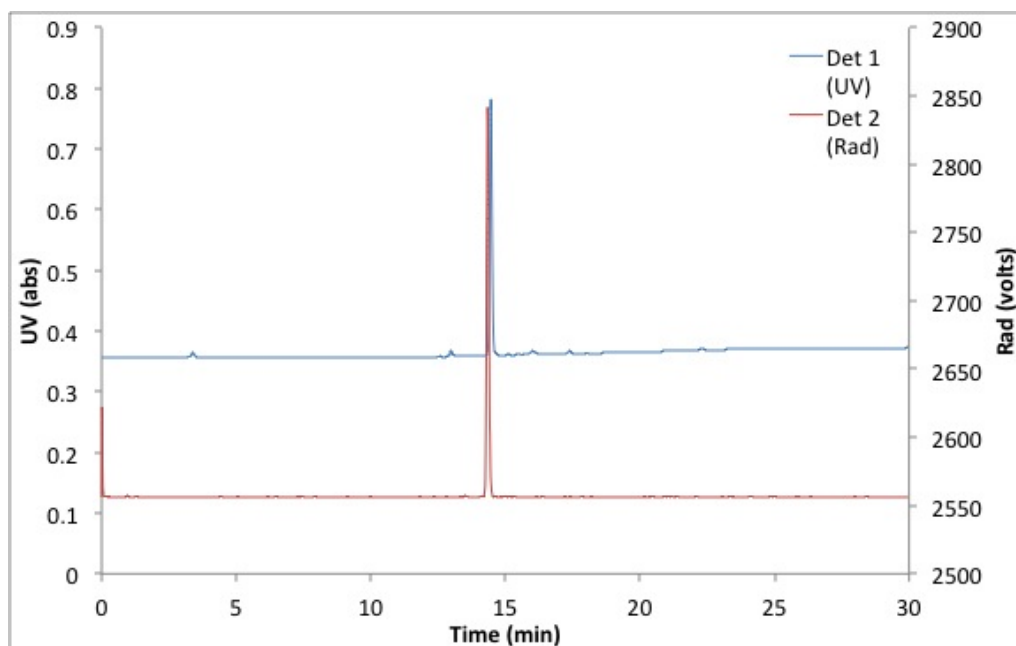


**Figure C.8:** Radio-HPLC spectrum for the product 1 three hours after synthesis, conducted on 2015/02/18, [ $^{211}\text{At}$ ]-MAP-1095

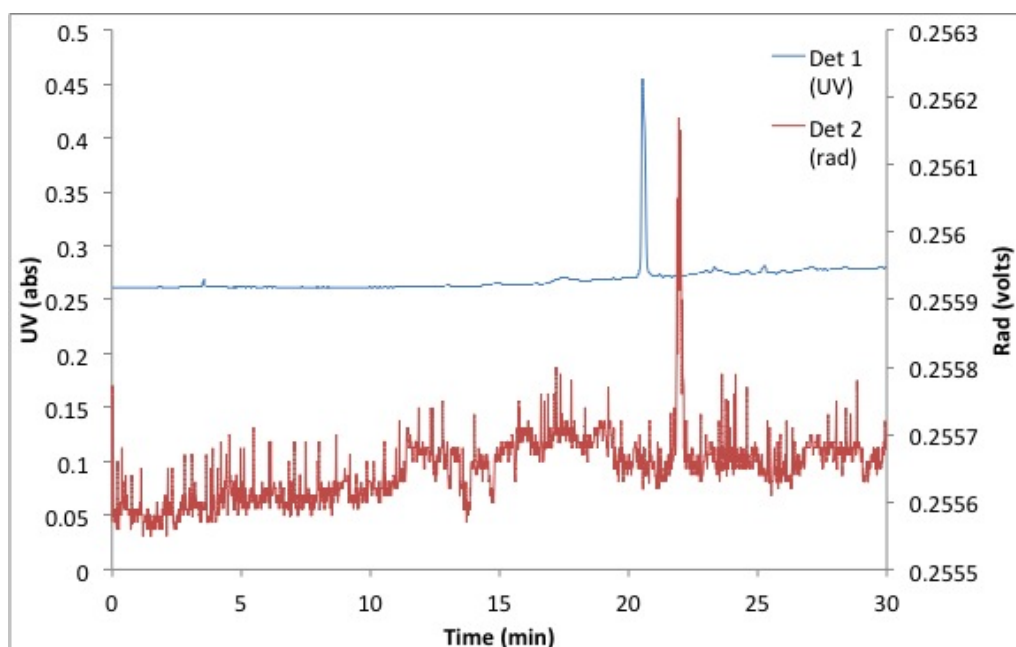


**Figure C.9:** Radio-HPLC spectrum for product 1 immediately after synthesis, conducted on 2015/03/04, [ $^{211}\text{At}$ ]-MAP-1095

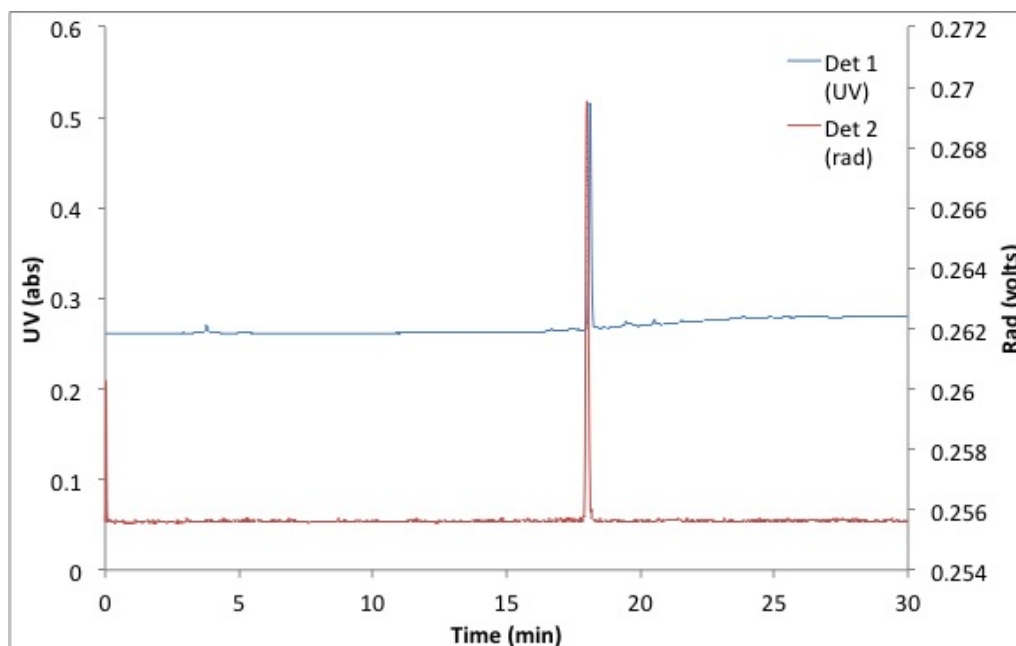


**Figure C.10:** Radio-HPLC spectrum for product 2 immediately after synthesis, conducted on 2015/03/04, [ $^{211}\text{At}$ ]-MAP-1095

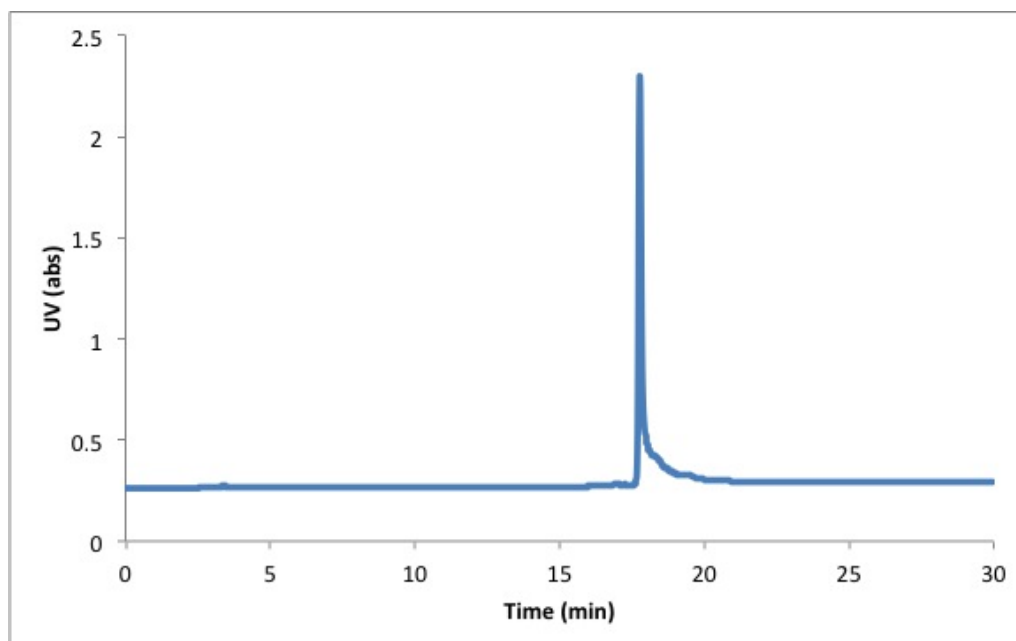


**Figure C.11:** HPLC spectrum for reference molecule before entering the column conducted on 2015/03/18, MIP-1095

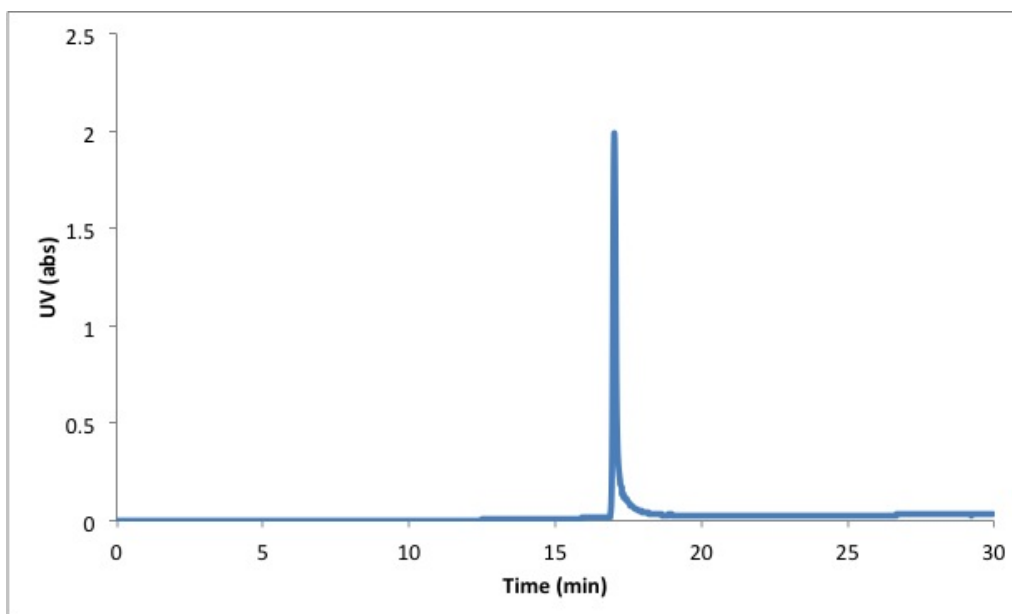


**Figure C.12:** HPLC spectrum for reference molecule before entering the column, a second verification, conducted on 2015/03/18, MIP-1095

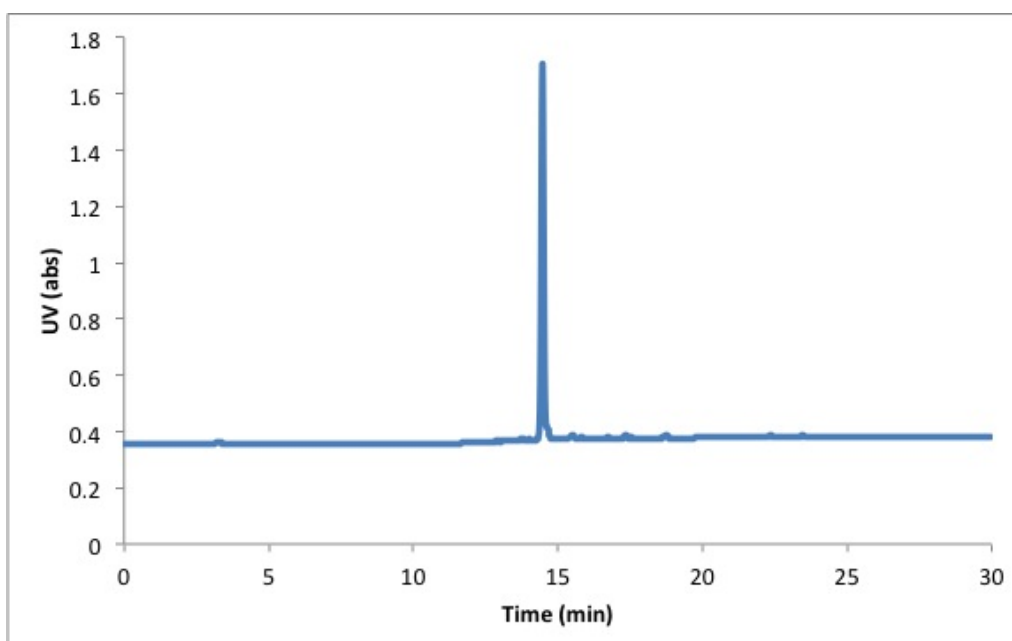


**Figure C.13:** HPLC spectrum for reference molecule after entering the column conducted on 2015/03/18, MIP-1095

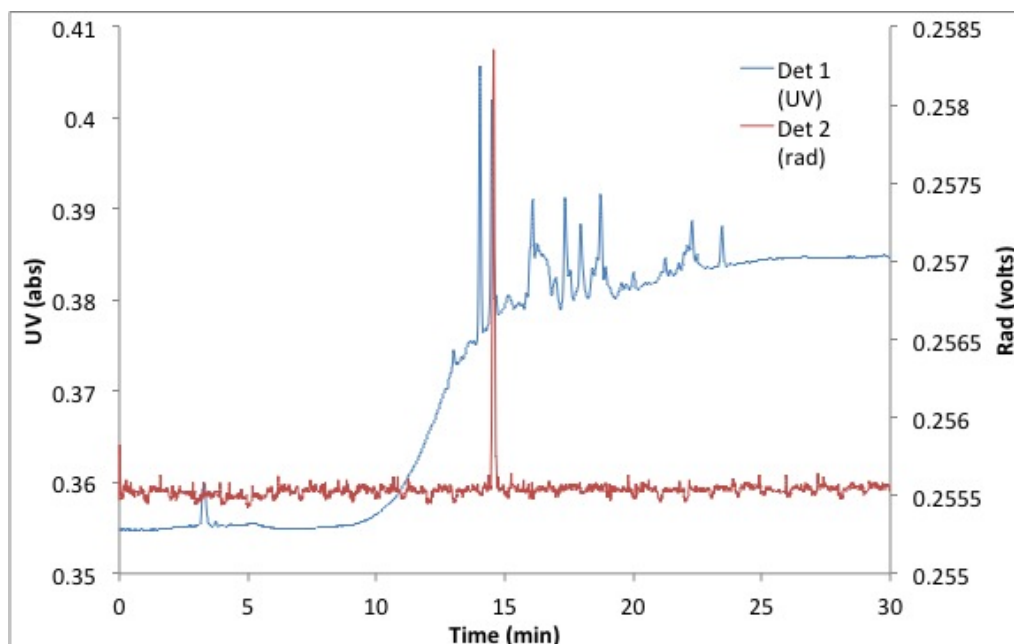


**Figure C.14:** Radio-HPLC spectrum for product 1 immediately after synthesis, conducted on 2015/03/18, [ $^{125}\text{I}$ ]-MIP-1095

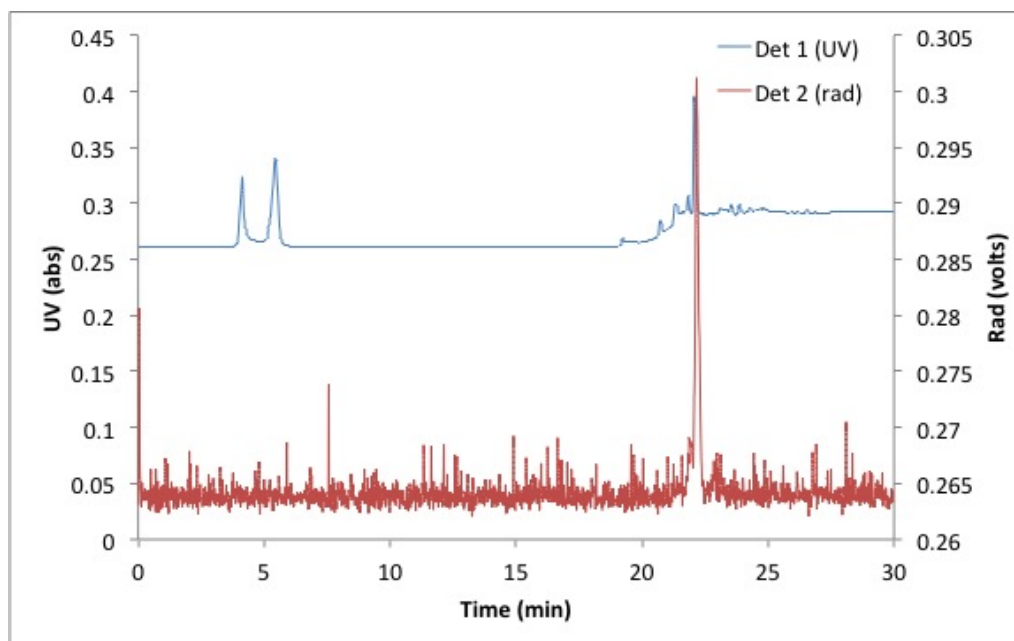


**Figure C.15:** Radio-HPLC spectrum for sample 1 immediately after synthesis, conducted on 2015/03/18, [ $^{125}\text{I}$ ]-MIP-1095

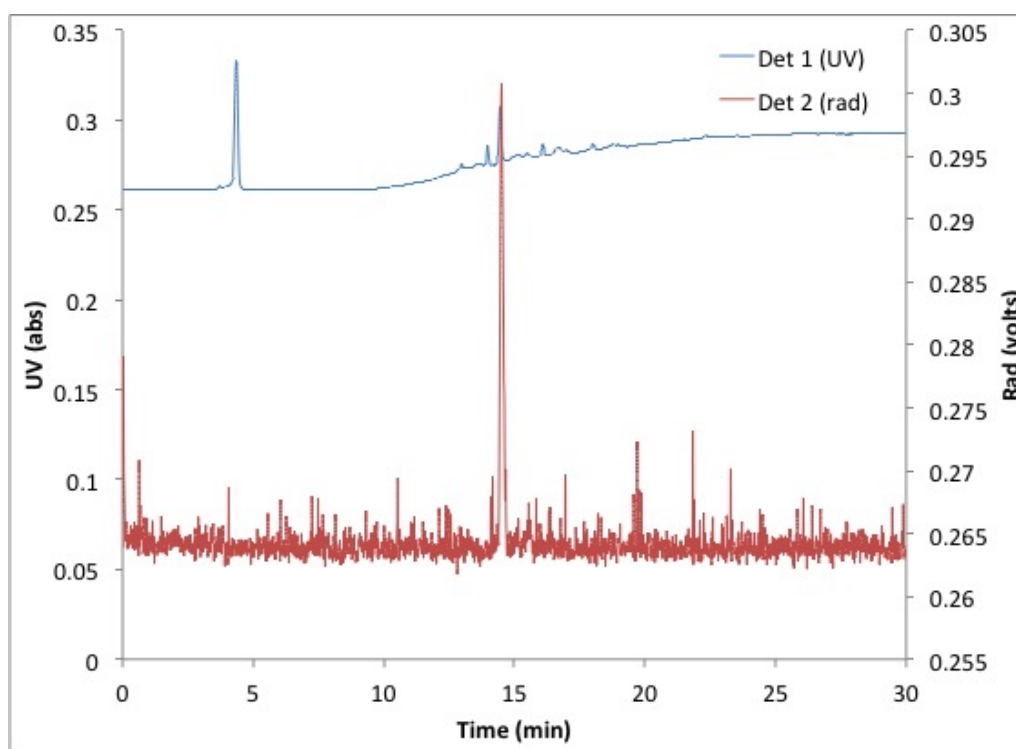


**Figure C.16:** Radio-HPLC spectrum for sample 2 immediately after synthesis, conducted on 2015/03/18, [ $^{125}\text{I}$ ]-MIP-1095

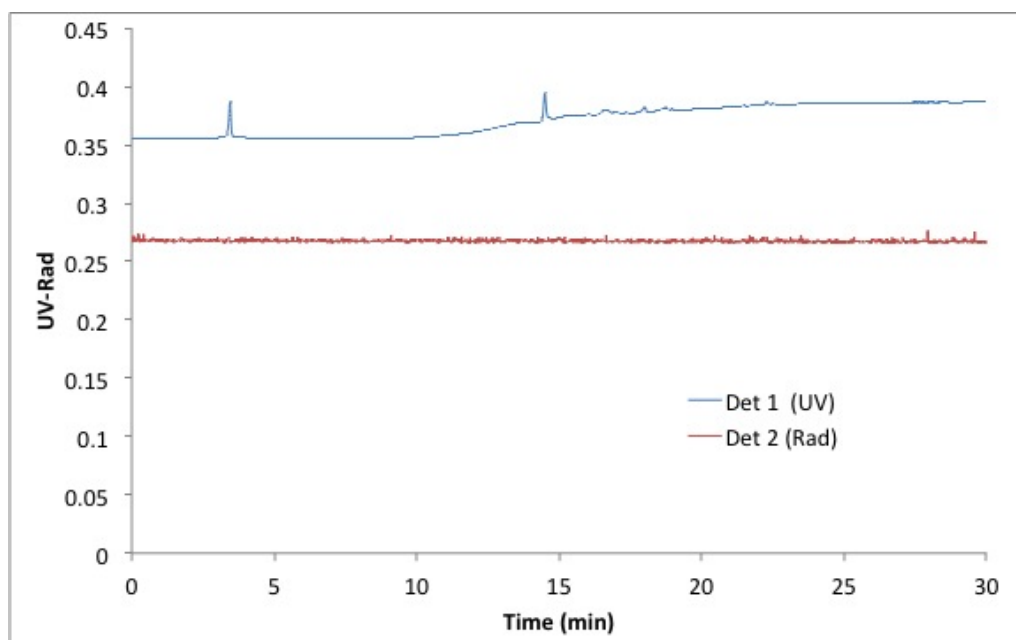


**Figure C.17:** Radio-HPLC spectrum for product 1 immediately after synthesis, conducted on 2015/03/25, [ $^{211}\text{At}$ ]-MAP-1095

### C. Radio-HPLC Spectra

---

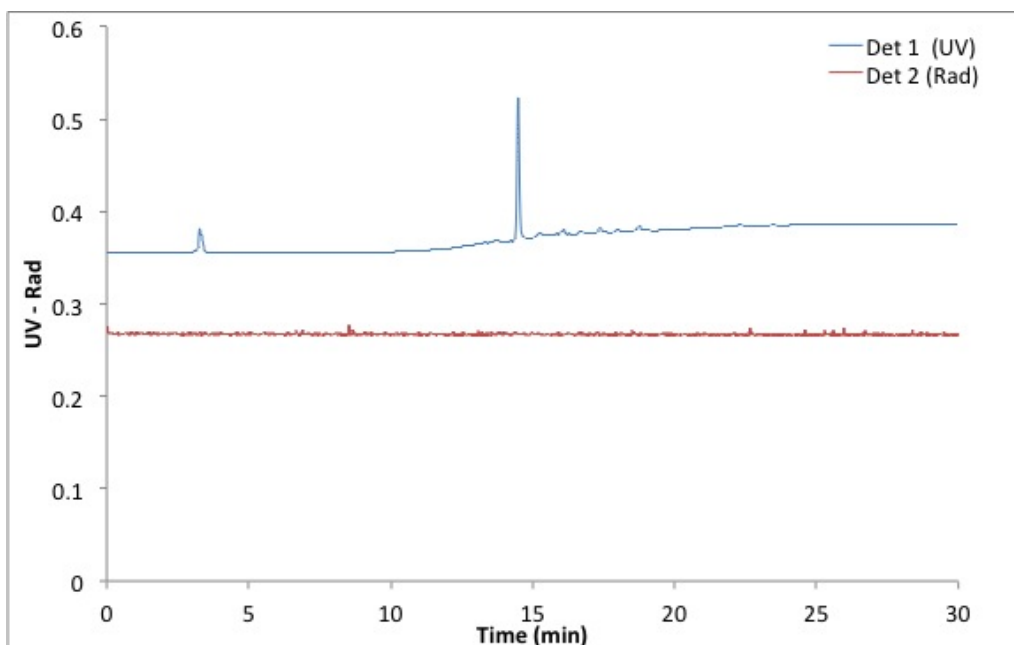


**Figure C.18:** Radio-HPLC spectrum for product 2 immediately after synthesis, conducted on 2015/03/25, [  $^{211}\text{At}$ ]-MAP-1095

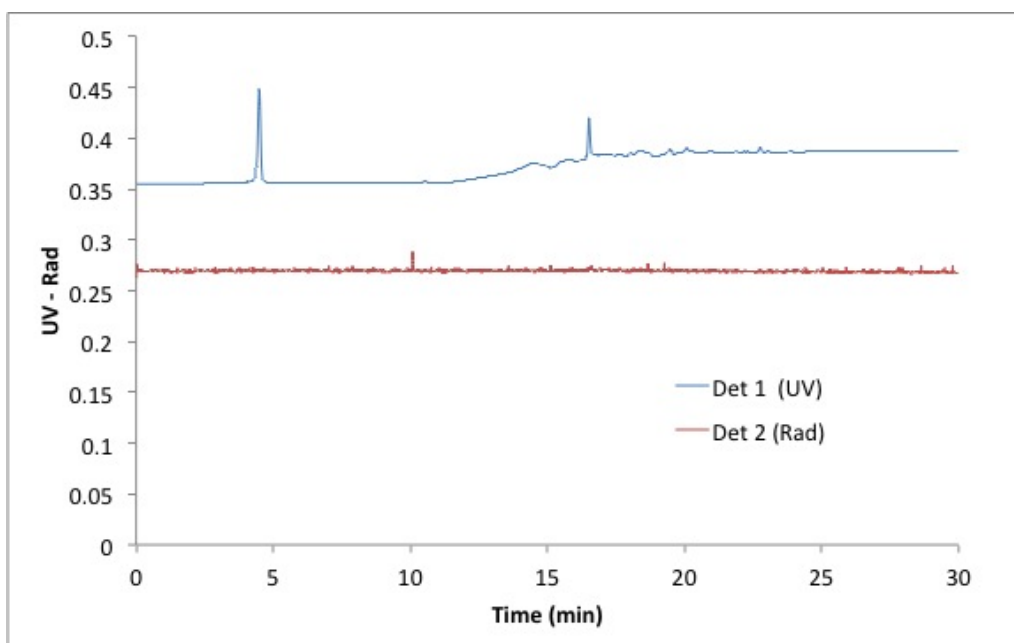


**Figure C.19:** Radio-HPLC spectrum for sample 1 immediately after synthesis, conducted on 2015/03/25, [  $^{211}\text{At}$ ]-MAP-1095

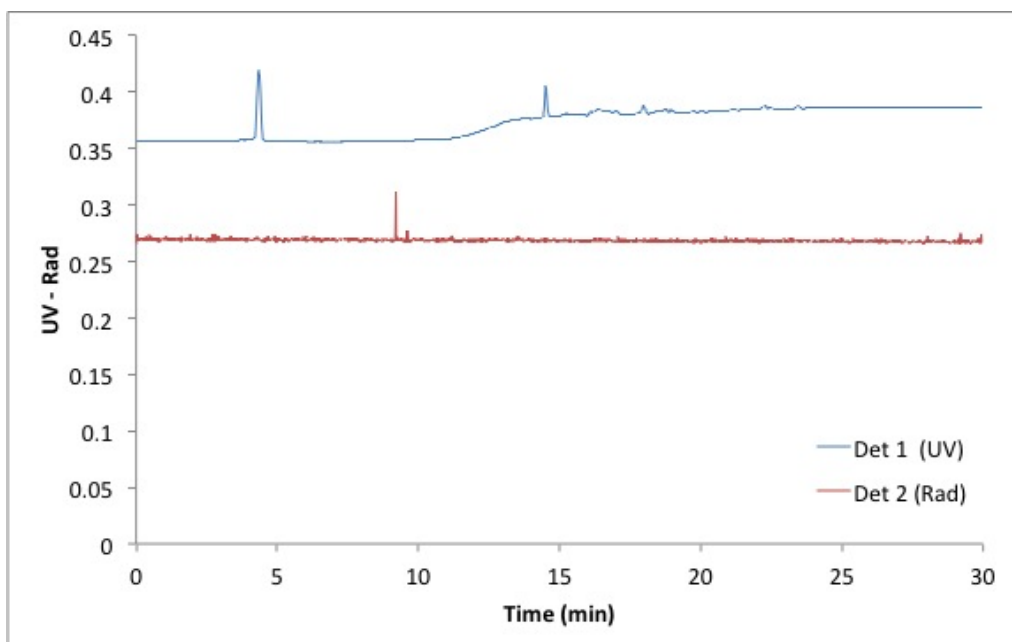


**Figure C.20:** Radio-HPLC spectrum for sample 2 immediately after synthesis, conducted on 2015/03/25, [ $^{211}\text{At}$ ]-MAP-1095

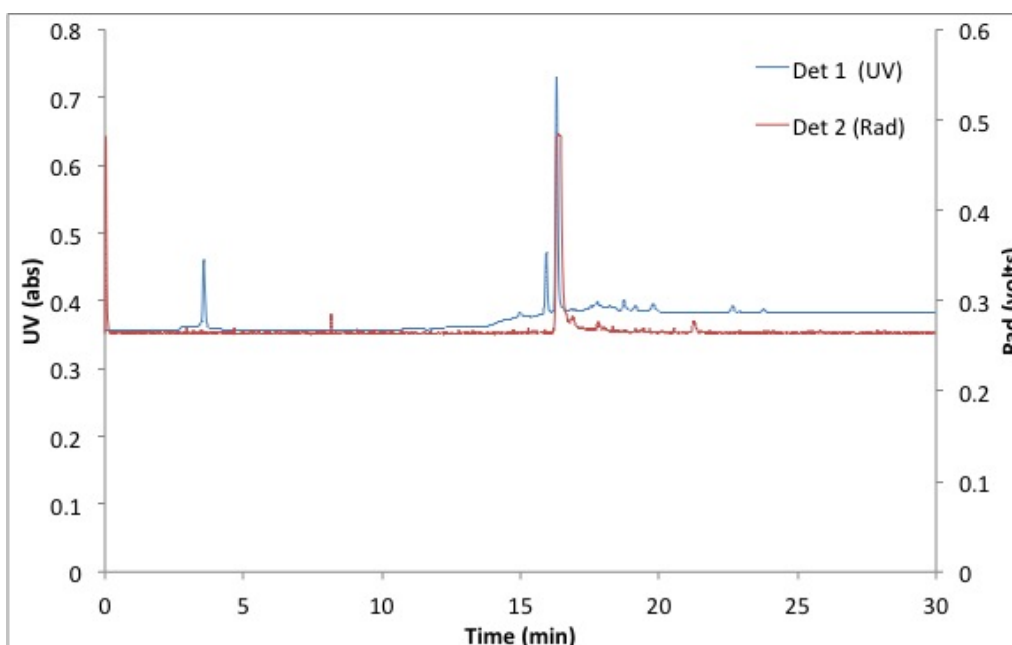


**Figure C.21:** Radio-HPLC spectrum for product 1 immediately after synthesis, conducted on 2015/03/27, [ $^{125}\text{I}$ ]-MIP-1095

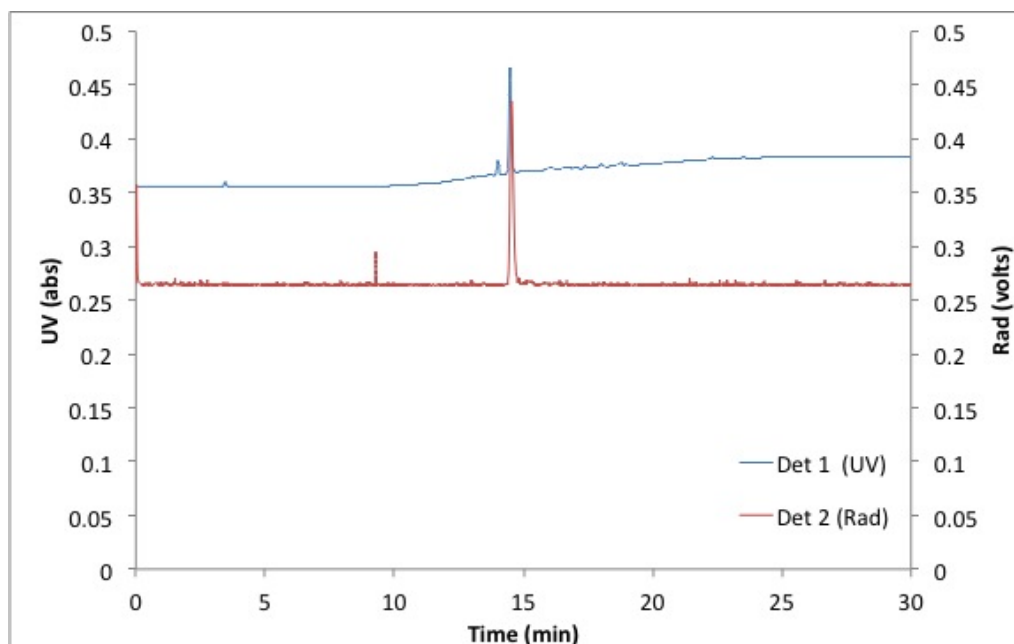


**Figure C.22:** Radio-HPLC spectrum for product 2 immediately after synthesis, conducted on 2015/03/27, [ $^{125}\text{I}$ ]-MIP-1095

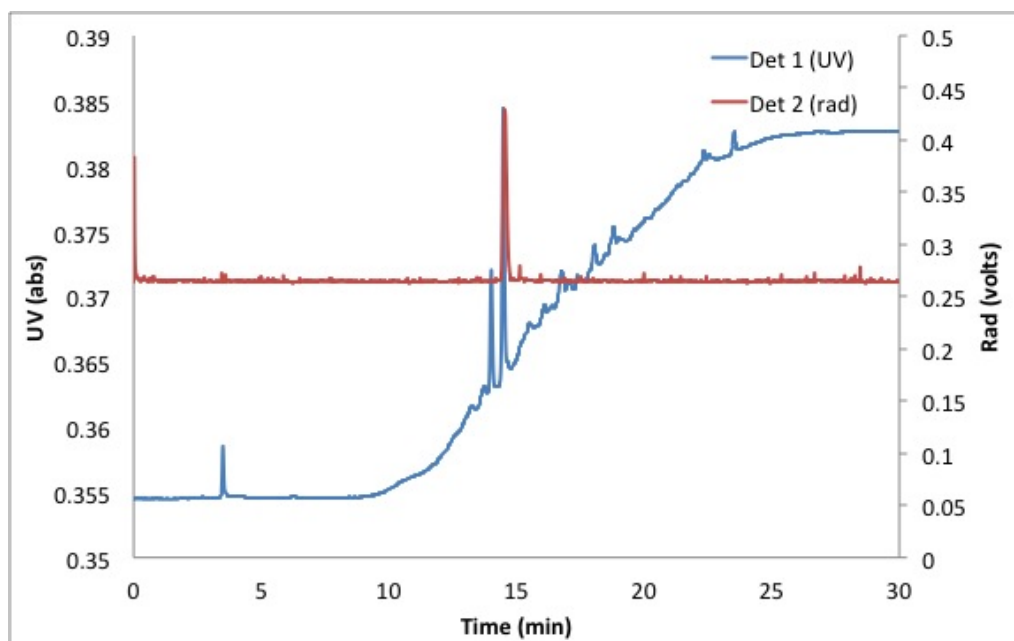


**Figure C.23:** Radio-HPLC spectrum for product 1 immediately after synthesis, conducted on 2015/04/01, [ $^{125}\text{I}$ ]-MIP-1095

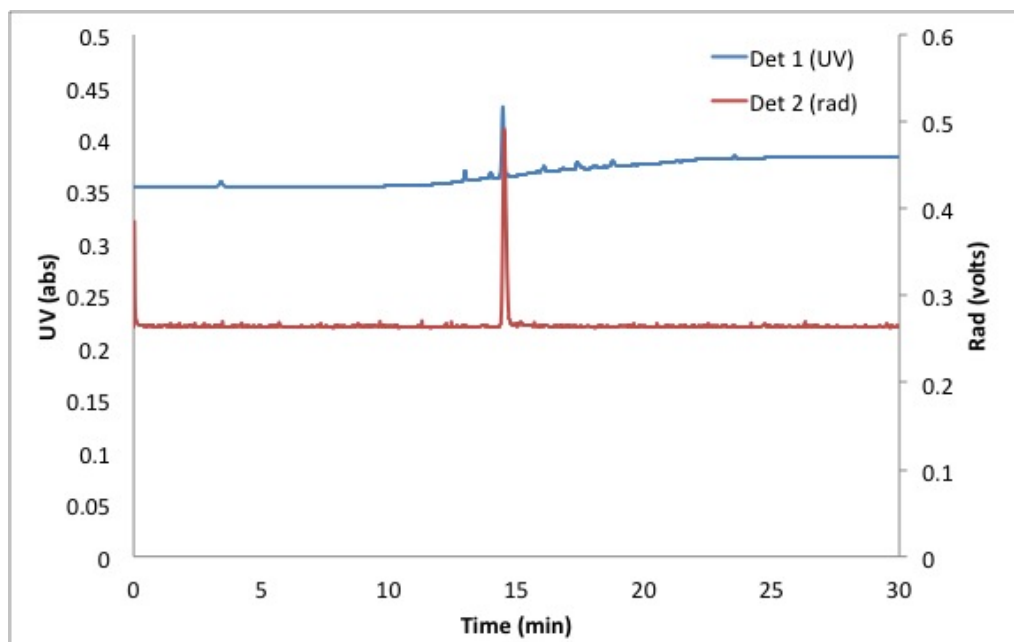


**Figure C.24:** Radio-HPLC spectrum for product 2 immediately after synthesis, conducted on 2015/04/01, [ $^{125}\text{I}$ ]-MIP-1095

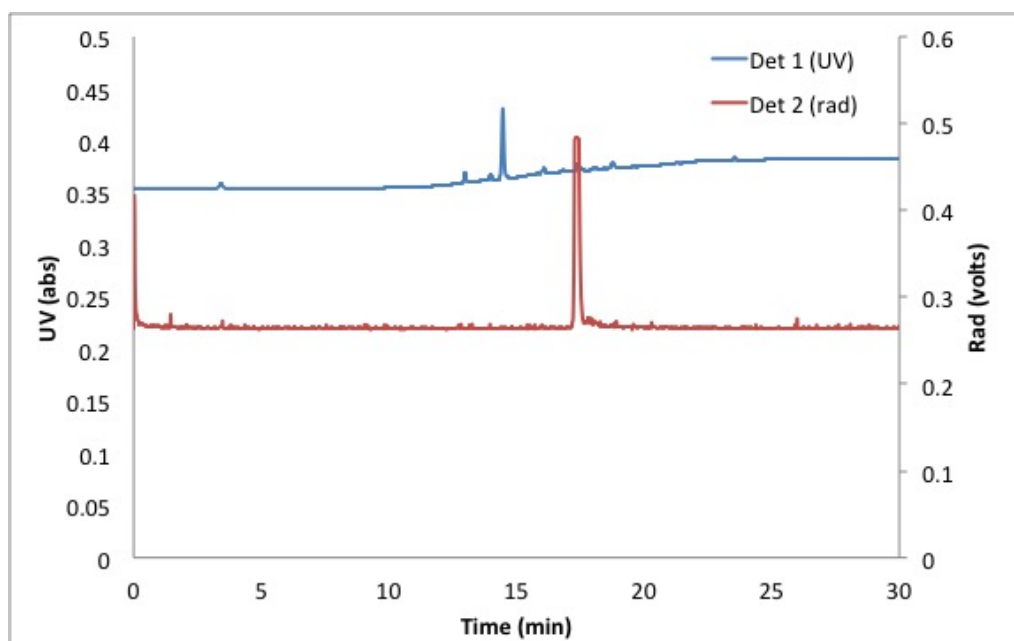


**Figure C.25:** Radio-HPLC spectrum for product 3 immediately after synthesis, conducted on 2015/04/01, [ $^{125}\text{I}$ ]-MIP-1095

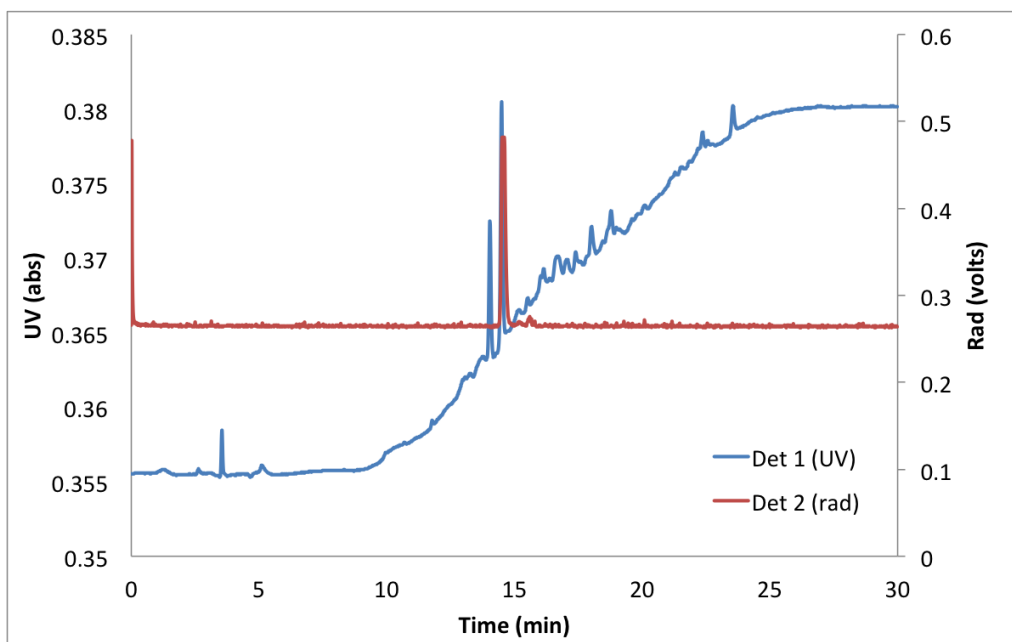


**Figure C.26:** Radio-HPLC spectrum for product 1 three weeks after synthesis, conducted on 2015/04/01, [ $^{125}I$ ]-MIP-1095

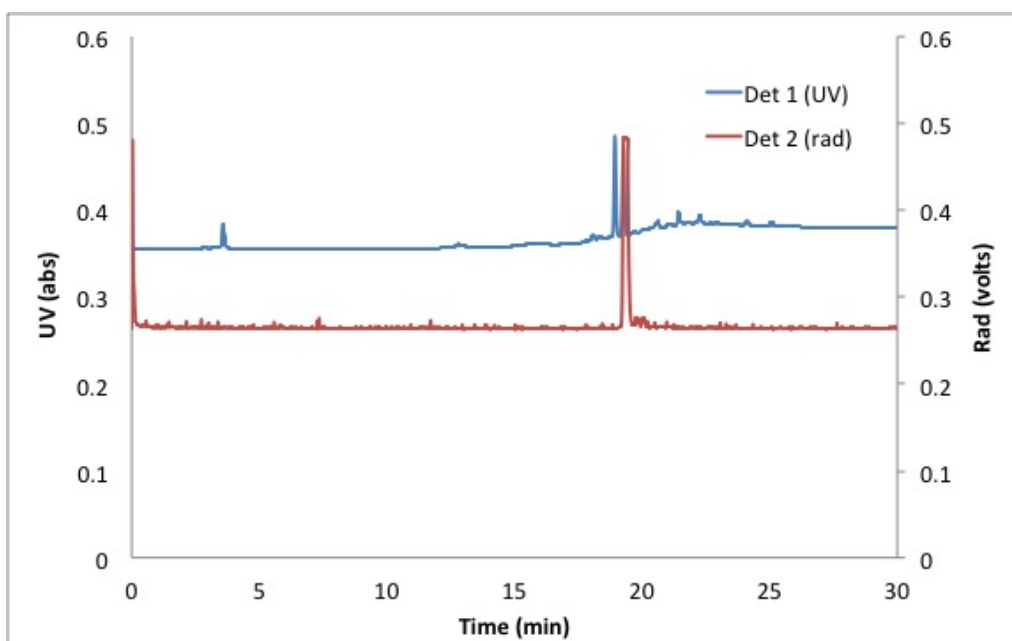


**Figure C.27:** Radio-HPLC spectrum for product 2 three weeks after synthesis, conducted on 2015/04/01, [ $^{125}I$ ]-MIP-1095

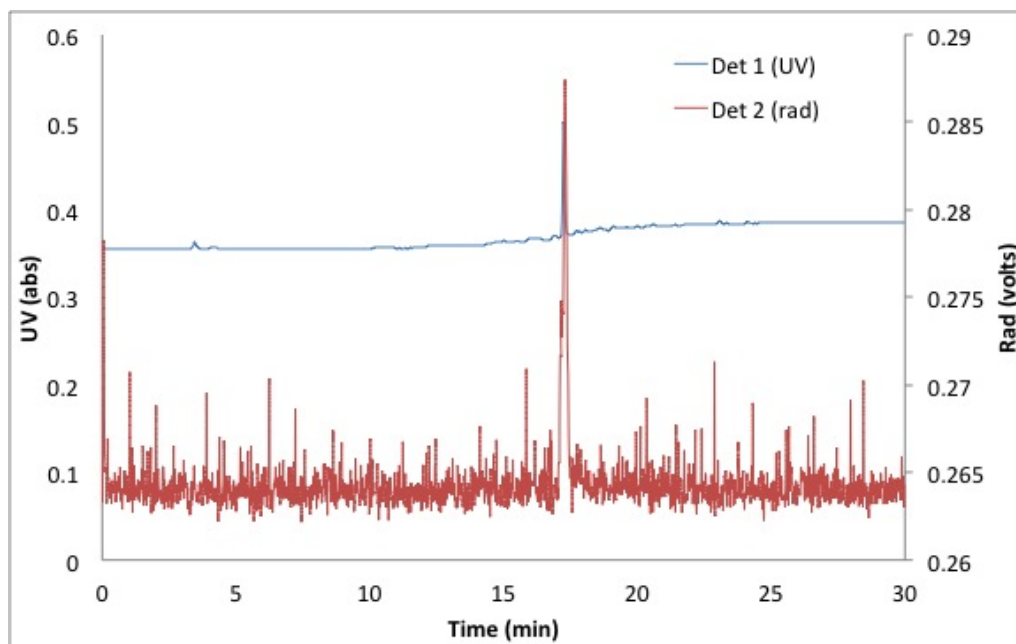


**Figure C.28:** Radio-HPLC spectrum for product 1 immediately after synthesis, conducted on 2015/04/08, [  $^{211}\text{At}$ ]-MAP-1095

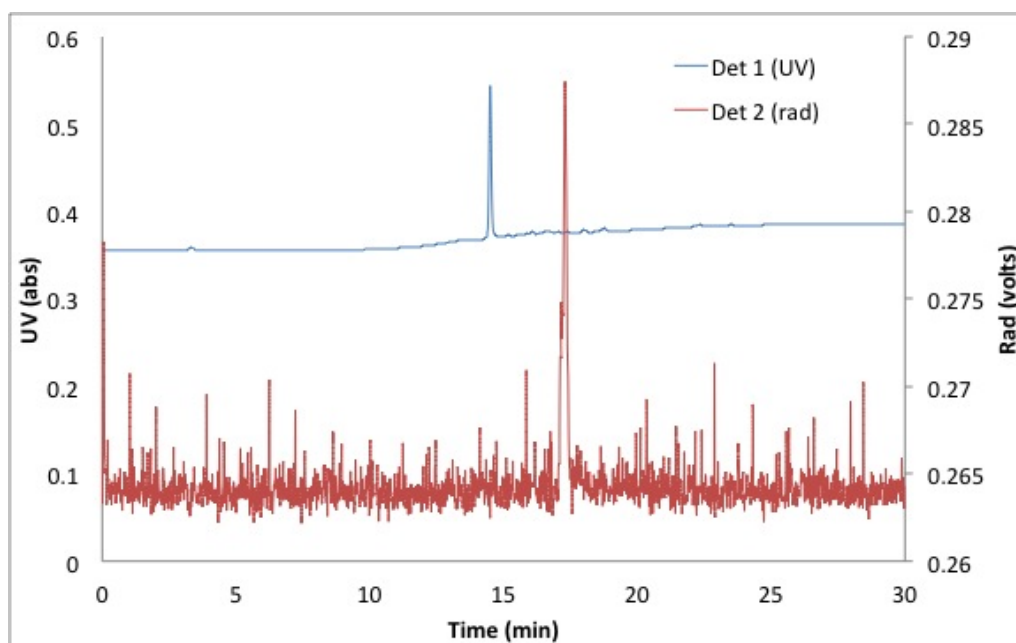


**Figure C.29:** Radio-HPLC spectrum for product 1 immediately after synthesis, conducted on 2015/04/08, [  $^{211}\text{At}$ ]-MAP-1095



# D

## Cell Binding

**Table D.1:** Comprehensive list of At-211 and I-125 cell binding experiments at room temperature

[C]	Position	Before		After		Stuck		B/T	
		Counts	CPM	Counts	CPM	Counts	CPM		
Stock	1	48787	98652.7	2733	5445.3	214	405.1	0.0576	0.0570
	2	48750	98574.1	3242	6464.8	199	373.8		
	3	45896	92744.7	2850	5681	149	274.3		
x5	4	9202	18418.8	2113	4205			0.2137	0.2124
	5	9374	18764.4	1891	3759.5				
	6	9168	18351.9	1926	3831				
x25	7	1886	3750.5	593	1161.9			0.3224	0.3177
	8	1860	3698.9	600	1175.9				
	9	1785	3546.9	590	1156.2				
Stock	1	130081	407786.4	33206	100686.1	1105	3291.9	0.2449	0.2371
	2	129721	406613.1	34207	103753.7	2114	6324.1		
	3	129234	405007.5	32212	97639.2	1138	3392.2		

**Table D.2:** Comprehensive list of I-125 cell binding experiments in an ice bath and at room temperature

	[C]	Position	Before		After		B/T	
			Counts	CPM	Counts	CPM		
Cold	Normal	1	841409	903292	59691	60057	0.0694	0.0634
		2	863290	957271	55820	56138		
		3	884726	983848	64259	64259		
	Diluted x5	4	179788	183364	31484	31570	0.1740	0.1710
		5	184126	187883	30264	30342		
		6	184255	188019	33620	33721		
Room Temp	Normal	7	868705	964013	69483	69992	0.0827	0.0751
		8	886244	985788	80736	81432		
		9	852193	943632	65480	65930		
	Diluted x5	10	184389	188165	58081	58431	0.3195	0.3144
		11	186736	190613	61132	61523		
		12	184769	188564	58419	58419		



# E

## Error Propagation

The error analysis was done for the specific activity following the GUM method using a Kratgen spreadsheet. The error for the RCY for labeling experiments and the  $B/T$  for the cell binding experience were found to be less 0.1% and are not reported here. The working equation for the specific activity is given in Equation E.1.

$$SA = \frac{A}{\frac{m_{ATE}}{V_{tot}} V_{exp}} \quad (\text{E.1})$$

$A$  is the activity of the  $^{125}I$  or the  $^{211}At$  eluted from the column,  $m_{ATE}$  is the mass of the ATE-P-1095 in the stock solution,  $V_{tot}$  is the total volume of the stock solution and  $V_{exp}$  is the volume of stock solution used in the experiment. The errors were assumed to be  $m_{ATE} = 0.0001g$  due to the scale,  $V_{tot} = V_{exp} = 1\%$  for properly calibrated micropipettes and  $A = \sqrt{counts}$ . Table E.1 contains a summary of the uncertainty analysis.

**Table E.1:** A summary of the uncertainties (unc), relative uncertainty (rel. unc.) and the range (U) in the specific activity (SA) calculations.

Trial	unc. (MBq/mg)	rel. unc. (%)	SA (MBq/mg)	U (k=2) (MBq/mg)
I-1	1.190	1.797	66.256	2.381
I-2	2.733	1.972	138.572	5.466
I-3	3.507	1.972	177.846	7.015
I-4	5.870	1.972	297.645	11.739
I-5	6.235	1.972	316.170	12.470
I-6	18.119	1.972	918.870	36.238
I-7	4.530	1.972	229.718	9.060
I-8	5.358	1.972	271.709	10.716
At-1	2.045	1.796	113.888	4.091
At-2	4.133	1.796	230.157	8.266
At-3	0.907	1.797	50.471	1.814
At-4	0.707	1.974	35.816	1.414
At-5	2.304	1.972	116.835	4.609
At-6	0.765	1.973	38.780	1.531
At-7	0.702	1.974	35.569	1.404
At-8	1.783	1.973	90.405	3.566
At-9	1.067	1.973	54.095	2.135